EVALUATION OF RESIDUAL STRESSES IN BIMETALLIC WELDS

A thesis submitted in partial fulfilment of the requirement for the award of degree

MASTER OF ENGINEERING
IN
PRODUCTION & INDUSTRIAL

Submitted By:
RAJESH
Roll No. 80782008

Under the Guidance of

Dr. Rahul Chhibber
Assistant Professor,
Deptt. Of Mechanical Engg.
Thapar University, Patiala
Patiala-147004

Dr. Bijan Kumar Dutta
Head,
Computational Mech. Section
Reactor Safety Division, BARC
Mumbai-400085

Ashwani Dhingra
Assistant Professer
Deptt. Of Mechanical Engg.
M.D.University,Rohtak

DEPARTMENT OF MECHANICAL ENGINEERING
THAPAR UNIVERSITY
PATIALA-147004, INDIA
June 2009

CERTIFICATE

This is to certify that the thesis titled, "Evaluation of Residual Stresses in Bimetallic Welds" being submitted by Mr. RAJESH, in partial fulfillment of the requirement for the award of degree of MASTER OF ENGINEERING (PRODUCTION & INDUSTRIAL) at THAPAR UNIVERSITY, PATIALA is a bonafied work carried out by his under our guidance and supervision and no part of this thesis has been submitted for the award of any other degree.

Dr. Rahul Chhibber
Assistant Professor,
Mecahnical Engineering Department,
Thapar University,
Patiala – 147004

Dr. Bijan Kumar Dutta
Head,
Computational Mech Section
Reactor Safety Division
BARC, Mumbai – 400085

Ashwani Dhingra
Assistant Professor
Deptt. of Mechanical Engg.
M.D.University, Rohtak

Countersigned by:

Dr. S.K. Mohapatra
Professor & Head,
Thapar University,
Patiala – 147004

Dr. R.K. Sharma
Dean, Academic Affairs
Thapar University,
Patiala – 147004

ACKNOWLEDGEMENT

I am highly grateful to the authorities of Thapar University, Patiala for providing this opportunity to carry out the seminar work.

I would like to express a deep sense of gratitude and thank profusely to my thesis guide Dr. Rahul Chhibber & Dr. Bijan Kumar Dutta for their sincere & invaluable guidance, suggestions and attitude which inspired me to submit seminar report in the present form.

I am also thankful to other faculty members of Mechanical Department, TU, Patiala for their intellectual support. My special thanks are due to my family members and friends who constantly encouraged me to complete this study.

RAJESH

ABSTRACT

Dissimilar metal joints between plates of mild steel and austenitic steel are widely used in various fields like nuclear power plant. failure analysis carried out on dissimilar joints and literature review have shown that a significant number of failure have occurred in the heat affected zone of the dissimilar welded joints residual stresses present in the welded joints are one of the main factors which cause failure in dissimilar welded joints.

In the present study mild steel and austenitic stainless steel AISI 304 were joined by the gas tungsten arc weld process using an austenitic stainless steel AISI 309 filler metal. A buttering layer of ER309 was laid on mild steel side to prevent carbon migration from mild steel to weld metal . Temperature measurement were determined by using the nickel and nickel & chrome thermocouples at various points on the dissimilar weld and obtained a profile w.r.t time . Residual stresses were determined in the dissimilar welded joints using stain gauge hole drilling method . Investigation was carried out to asses' residual stresses in different zones in weld coupons.

Tensile test, impact test , chemical composition test were also performed to check the ultimate tensile strength ,yield strength, impact strength, change in composition of weld metal .

Micro hardness, microstructure were carried out at different zones of the specimen with different parameters .different zones were heat affected zones ,base metals, fusion line weld centre and buttering layer.

Sr. no	LIST OF FIGURES	Page no
1	Complete stress relaxation technique	11
2	Strain gauge rosette for the hole of a typical three element drilling.	13
3	Diffraction produced by reflections from adjacent atomic planes	16
4	Schematic diagram of setup for X ray diffraction technique	18
5	Process diagram of tungsten inert gas welding	19
6	Gas tungsten arc welding	20
7	Power source for TIG WELDING machine	21
8	wire spool arrangements	21
9	Shows the gas flow rate of shielding gas	26
10	TIG welding process	27
11 11.1	Groove Design	36 38
12	Mountings of thermocouples at different points	39
13	Mountings of nickel& nickel chromium thermocouples in weld coupon	39
14	Arrangement of recording of temperature in bimetallic weld	41
15	Mounting of strain gauge in weld coupon	43
16	Show the drilling operation during the stress relaxation techniques	43
17	Show the data taker recording the strain	47
18	Temperature profile for coupon 1 at various points of measurement	47
19	Mean temperature profile for coupon 1 at different points	48
20	Peak temperature profile for coupon 1	49
21	Temperature profile for coupon 2 at various points of measurement	49
22	Mean temperature profile for coupon 2 at various points of measurement	50
23	Peak temperature profile for coupon 2	50
24	Load displacement graph for coupon 1	51
25	Load displacement graph for coupon 1	51
26	Load displacement graph for coupon 2	52
26.1	Load displacement graph for coupon 1	52
27	Toughness of weld coupon 1	53
28	Toughness of weld coupon 2	54
29	Longitudinal residual stresses for coupon 1	55
30	Transverse residual stresses for coupon 1	56
31	Longitudinal residual stresses for coupon 2	57
32	Transverse stress for coupon 2	57
33	Relation between long. stresses & temp. at different of coupon 1	58
34	Relation between longitudinal stresses & temperature at different	58

CHAPTER 1 INTRODUCTION

1.1 WELDING PROCESS

Rapid development and improvement of welding techniques, driven by the need for low cost and weight saving, there is a potential trend to replace rivets and fasteners with welds in connection of structural components.

The advantages of welding, as a joining process, include high joint efficiency, simple set up, flexibility and low fabrication costs. Even though it has many positive properties, fusion welding can alter the properties of the material and may causes deflection, shrinkage and/or residual stresses in the joint. A post weld heat treatment is widely used to relieve the residual stresses caused by welding

The welding process is used in almost all industries. The circumferential butt-weld is a common type of joint in stainless steel piping systems in power plant. Owing to the relatively large wall thickness in such piping systems, butt-weld is often constructed of several weld passes. Due to the intense concentration of heat in the welding, the regions near the weld line undergo severe thermal cycles. The thermal cycles cause non-uniform heating and cooling in the material, thus generating inhomogeneous plastic deformation and residual stresses in the weldment. The presence of residual stresses can be detrimental to the performance of the welded product. Tensile residual stresses are generally detrimental, increasing the susceptibility of a weld to fatigue damage, stress corrosion cracking and fracture [1]. When assessing the risk for growth of defects such as surface flaws in piping systems the welding residual stress may give a large contribution to the total stress field than stress caused by design loads [2]. Moreover, in order to prevent inter-granular stress corrosion cracking in the root area of welds in stainless steel, it is necessary to satisfy certain requirements concerning process condition, material properties and welding residual stress. Therefore, a good estimation of the welding residual stress field is then needed.

The distribution of welding residual stress depends on several main factors such as structural dimensions, material properties, restraint conditions, heat input, number of weld pass and welding sequence. Hence, for multi-pass welding the welding residual stresses may be very complex, and it is very difficult to predict the distribution of welding residual stress due to the multi-pass welding operation.

1.2 BIMETALLIC WELD

In the power generation industry, various components/ systems operate at different service conditions and hence appropriate materials are used for these components/ systems. Components operating at high temperatures are made of stainless steels and those operating at lower temperatures are made of ferritic steels. Therefore, dissimilar joints are inevitable for linking the components/systems made of different materials, for example, dissimilar metal joints between pipes of ferritic steels and austenitic stainless steels are used in steam generators. The dissimilar metals joints are prone to frequent failures [3–12] and these failures are generally attributed to one or more of the following causes: (a) difference in mechanical properties across the weld joint and coefficients of thermal expansion (CTE) of the two types of steels (CTE for austenitic SS and ferritic steel are typically 18 and 14!10K6/K, respectively) and the resulting creep at the interface [13,14], (b) general alloying problems of the two different base metals [15,16] such as brittle phase formation and dilution, (c) carbon migration from the ferritic steel into the stainless steel [4,13], which weakens the HAZ in the ferritic steel, (d) preferential oxidation at the interface [17–18], (e) residual stresses present in the weld joints (f) service conditions and other factors [19–20] etc.

Operating experience with dissimilar weld joints has also shown that a significant number of failures occurred in less than the expected service life [21]. A majority of the transition joint failures in austenitic/ferritic steels joints occur in the heat affected zone (HAZ) of the ferritic steel, adjacent to the weld interface. In power plants, there is strong evidence that residual stress is a major cause of cracking in welds and HAZ regions during service [14, 22]. These joints involve the use of an intermediate Inconel-82 buttering on the ferritic steel and stress relief heat treatment (SRHT) at 998 K (725 8C) prior to the fill-up of the weld joint.

There are many methods to evaluate the residual stress distribution. Previously, welding residual stress analysis used only experimental measurement methods. These methods can be divided into two categories. One is destructive method. For instance, Pang and Pukas [23] measured stresses by hole drilling and strain gauge techniques. The other is non-destructive method. For example, Chandra [24] and Brand [25] measured residual stresses in a weld bead by X-ray diffraction (XRD) techniques; Chu [26] measuredwelding residual stresses using supersonic waves. The XRD method is highly accurate, but is limited by the fact that only information is obtained about a relatively thin surface layer (27).

1.3 RESIDUAL STRESSES

Residual stresses can be defined as those stresses that remain in a material or body after manufacture and processing in the absence of external forces or thermal gradients.

Due to the intense concentration of heat in the welding, the regions near the weld line undergo severe thermal cycles. The thermal cycles cause non-uniform heating and cooling in the material, thus generating inhomogeneous plastic deformation and residual stresses in the weldment. The presence of residual stresses can be detrimental to the performance of the welded product. Tensile residual stresses are generally detrimental, increasing the susceptibility of a weld to fatigue damage, stress corrosion cracking and fracture [28]. When assessing the risk for growth of defects such as surface flaws in piping systems the welding residual stress may give a large contribution to the total stress field than stress caused by design loads [29]. Moreover, in order to prevent inter-granular stress corrosion cracking in the root area of welds in stainless steel, it is necessary to satisfy certain requirements concerning process condition, material properties and welding residual stress. Therefore, a good estimation of the welding residual stress field is then needed.

The distribution of welding residual stress depends on several main factors such as structural dimensions, material properties, restraint conditions, heat input, number of weld pass and welding sequence. Hence, for multi-pass welding the welding residual stresses may be very complex, and it is very difficult to predict the distribution of welding residual stress due to the multi-pass welding operation [30].

Residual stresses, which appear during different stages of the manufacturing process of structural elements or their operating, may exert a considerably negative influence on both the structure’s static strength and fatigue life-time. On the other hand, taking into account actual residual stress distributions often reveals new beneficial operating capabilities for some types of structural units. In particular, recent trends are directed toward a substitution of traditional pin or rivet joints of airframe components with analogous welded joints.

1.3.1 TYPES OF RESIDUAL STRESSES

.Residual stresses may be categorized by cause (e.g. thermal or elastic mismatch), by the scale over which they self-equilibrate, or according to the method by which they are measured [31]. Residual stresses can be defined as either macro or micro stresses and both may be present in a component at any one time. Macro residual stresses, which are often

referred to as Type I residual stresses, vary within the body of the component over a range much larger than the grain size. Micro residual stresses, which result from differences within the microstructure of a material, can be classified as Type II or III. Type II residual stresses are micro residual stresses that operate at the grain-size level; Type III are generated at the atomic level [32].

Micro residual stresses often result from the presence of different phases or constituents in a material. They can change sign and/or magnitude over distances comparable to the grain size of the material under analysis. To summarize, residual stresses can be classified as:

Type I - which refer to macro residual stresses that develop in the body of a component on a scale larger than the grain size of the material

Type II-are micro residual stresses that vary on the scale of an individual grain.Such stresses may be expected to exist in single-phase materials because of anisotropy in the behavior of each grain.

Type II They may also develop in multi-phase materials because of the different properties of the different phases are micro residual stresses that exist within a grain, essentially as a result of the presence of dislocations and other crystalline defects.

Types II and III are often grouped together as micro stresses. When comparing results from different techniques, consideration should be given to the sampling volume and resolution of each measurement method in relation to the type of residual stress being measured, particularly when the Type II and III micro residual stresses are of interest. It is important also to consider the concept of the characteristic volume, which can be used to describe the volume over which a given type of residual stress averages to zero. Most material removal techniques (e.g. hole drilling, layer removal) remove large volumes of material over which Type II and III stresses average to zero so that only the macro residual stresses can be measured [31,32].

1.3.2 Origins

Residual stresses develop during most manufacturing processes involving material deformation, heat treatment, machining or processing operations that transform the shape or change the properties of a material. They arise from a number of sources and can be present in the unprocessed raw material, introduced during manufacturing or can arise from in-service loading [31]. The origins of residual stresses in a component may be classified as:

a) Mechanical

b) Thermal

c) Chemical

a) Mechanically Generated Residual Stresses

Mechanically generated residual stresses are often a result of manufacturing processes that produce non-uniform plastic deformation. They may develop naturally during processing or treatment, or may be introduced deliberately to develop a particular stress profile in a component [31]. Examples of operations that produce undesirable surface tensile stresses or residual stress gradients are rod or wire drawing (deep deformation), welding, machining (turning, milling) and grinding (normal or harsh conditions). Compressive residual stresses usually lead to performance benefits and can be introduced by shot peening, auto-frettage of pressure vessels, toughening of glass or cold expansion of holes.

b) Thermally Generated Residual Stresses

On a macroscopic level, thermally generated residual stresses are often the consequence of non-uniform heating or cooling operations. Coupled with the material constraints in the bulk of a large component this can lead to severe thermal gradients and the development of large internal stresses. An example is the quenching of steel or aluminium alloys, which leads to surface compressive stresses, balanced by tensile stresses in the bulk of the component

c) Chemically Generated Residual Stresses

The chemically generated stresses can develop due to volume changes associated with chemical reactions, precipitation, or phase transformation. Chemical surface treatments and coatings can lead to the generation of substantial residual stress gradients in the surface layers of the component. Nitriding produces compressive stress in the diffusion region because of expansion of the lattice and precipitation of nitrides, and carburising causes a similar effect. The magnitude of residual stresses generated in coatings can be very high compressive stresses of the order of 6-8GPa or higher have been measured at the interface of some thermal barrier coatings (TBCs) [31].

1.3.3 Equilibrium Condition of Residual Stresses

Because residual stresses exist without external force, the resultant force and the resultant moment produced by the residual stresses must vanish on any plane section

$$\int \sigma.dA = 0$$

$$\int dM = 0$$

Where dA is area and dM is the resultant moment [33].

1.3.4 Effect of Residual Stresses

Residual stresses adversely affect the service behavior of the structure. Their effect is subtle, far-reaching, and occasionally disastrous. High tensile residual stresses in regions near the weld may produce brittle fracture, fatigue or stress corrosion cracking. Stress corrosion cracking and hydrogen induced cracking of a weldment can occur without any external loading in the presence of residual stresses. A significant detrimental effect of residual stresses is the intergranular stress corrosion cracking in austenitic stainless steel. In addition such stresses appear to accelerate all forms of corrosion.

Compressive residual stresses and initial distortion may reduce the buckling strength. Since in regions where both the residual and applied stresses are compressive they are additive, so that the critical applied load will be lower in the presence of such a residual stress system than if there were no residual stresses.

The Residual stresses influence the fatigue behavior of the welded assemblies because the local stresses result from the superposition of welding residual stresses and of the variable stresses in service. When compressive residual stresses exist in regions near the surface of a plate, the fatigue strength may be increased. Residual stresses are of yield-point magnitude at room temperature that would cause preferential creep, highly localized at the weld region, and in due course give rise to premature failure [32].

Residual stress is not only governed by the magnitude and distribution but also by the brittleness of the material. When the material is brittle, residual stresses can reduce the fracture strength of the weldment significantly. On the other hand, when the material is ductile the effects of residual stresses on fracture are negligible [34, 35].

On the other hand, residual stresses can be useful and intentionally induced as in auto-frettage. This process involves over straining the tube or pressure vessel, by application of high internal pressure. The material at the inner surface yields with the plastic deformation penetrating deeper and deeper into the cylinder wall as the pressure is increased. The compressive stresses thus induced increase the pressure that can be sustained by cylinder in service [36].

1.3.5 Chief Factors Responsible for Setting up of Residual Stresses

1. Qualities of the parent metal and filler rod or electrode,
2. Shape and size of weld,
3. Comparative weights of weld metal and parent metal,
4. Type of joint and method used in making weld (e.g. tacking, back-step sequence, etc.)
5. Heat input into the weldment i.e. on flame size in oxyacetylene welding; and current, electrode size and welding speed in arc welding,
6. Type of structure and neighbouring joints,
7. Expansion and contraction (free or constrained component),
8. Rate of cooling,
9. Stresses already present in the weld metal [36].

1.3.6 Methods of Relieving or Controlling Welding Residual Stresses

Residual stresses are virtually elastic deformations which posses some potential energy accumulated in a body. The main feature of residual stress relieving is that they can be avoided only through metal plastic deformation, where, how and when to develop deformation are important points of the problem. The choice of residual stress relieving method greatly depends on the kind of residual stresses and its negative effect on the weld structure. Reducing welding Residual stresses consists, of the following possibilities:

(i) Decreasing the level of residual stresses, in particular the maximum tensile stress level,

(ii) Decreasing the zones with high residual stresses,

(iii) Decreasing the degree of multi-axiality of residual tensile stresses.

To achieve these aims the following methods are employed:

(i) Design consideration

(ii) Material consideration

(iii) Heat treatment

(iv) Mechanical stress relieving process

(a) Shot peening

(b) Hammer peening

(v) Vibration stress relief

(vi) Explosive treatment.

1.3.7 Residual Stress Measuring Techniques

Classification of techniques for measuring residual stresses:

Many techniques have been proposed and used for measuring residual stresses in metals.

Table 1 classifies presently available techniques, they are:

a) Stress relaxation techniques,

b) X-Ray Diffraction techniques.

c) Techniques using stress sensitive properties.

d) Cracking techniques.

Table: 1 Classification of techniques for measuring residual stresses

A-1 Stress-relaxation techniques using electric and mechanical strain gages	Techniques applicable primarily to plates	1. Sectioning technique using electric resistance strain gages 2. Gunnert technique 3. Mathar-Soete drilling technique 4. Stäblein successive milling technique
	Techniques applicable primarily to solid cylinders and tubes	5. Heyn-Bauer successive machining technique 6. Mesnager-Sachs boring-out technique
	Techniques applicable primarily to three-dimensional solids	7. Gunnert drilling technique 8. Rosenthal-Norton sectioning technique
A-2 Stress-relaxation techniques using apparatus other than electric and mechanical strain gages		9. Grid system-dividing technique 10. Brittle coating-drilling technique 11. Photoelastic coating-drilling technique
B X-ray diffraction techniques		12. X-ray film technique 13. X-ray diffractometer technique
C Techniques using stress-sensitive properties	Ultrasonic techniques	14. Polarized ultrasonic wave technique 15. Ultrasonic attenuation technique
		16. Hardness techniques
D Cracking techniques		17. Hydrogen-induced cracking technique 18. Stress corrosion cracking technique

In the stress relaxation techniques, residual stresses are determined by measuring elastic strain release. This takes place when residual stresses are relaxed by cutting the specimen into pieces or by removing a piece from the specimen. Strain released during stress relaxation can be determined using a grid system, brittle coatings or photo-elastic coatings or electrical or mechanical strain gauges.

Elastic strains in metals that have crystalline structures can be determined by measuring the lattice parameters using X-Ray Diffraction techniques. Since lattice parameters of a metal in the unstrained state is known or can be determined separately, elastic strains in the metal can be determined non-destructively without machining or drilling.

Attempts have been made to determine residual stresses in metals by measuring stress sensitive properties. Proposed stress measuring techniques include ultrasonic and hardness methods [37].

The most widely used techniques are discussed below.

a) Stress Relaxation Techniques

The stress relaxation techniques are based on the fact that strains taking place during unloading are elastic even when the material has undergone plastic deformation.

1. Sectioning Technique for a Plate using Elastic Resistance Strain Gauges

Using this technique, electrical resistance strain gauges are mounted on the surface of the test structure or specimen. A small piece of metal containing the gauges is then removed from the structure, as shown in Fig.1, measuring is made of strain changes, εx, εy , and yxy , that take place during the removal of the piece.

$$\bar{\varepsilon}_x = -\bar{\varepsilon}_x'$$

$$\bar{\varepsilon}_y = -\bar{\varepsilon}_y$$

$$\bar{\gamma}_{xy} = -\bar{\gamma}_{xy}$$

Where , εx,εy,and yxy are elastic strain components of the residual stress. The minus signs indicate that, when tensile residual stresses exist, shrinkage (not elongation) takes place during stress relaxation. Then residual stresses

$$\sigma_x = -\frac{E}{1-\nu^2}\left(\bar{\varepsilon}_x + \nu\bar{\varepsilon}_y\right)$$

$$\sigma_y = -\frac{E}{1-\nu^2}\left(\bar{\varepsilon}_y + \nu\bar{\varepsilon}_x\right)$$

$$\tau_{xy} = -G\bar{\gamma}_{xy}$$

It is advisable to make strain measurements on both surfaces of the plate because residual stresses may be caused by bending. The mean value of strains measured on both surfaces represents the plane stress component, while the difference between the strains on both surfaces represents the stress component caused by bending.

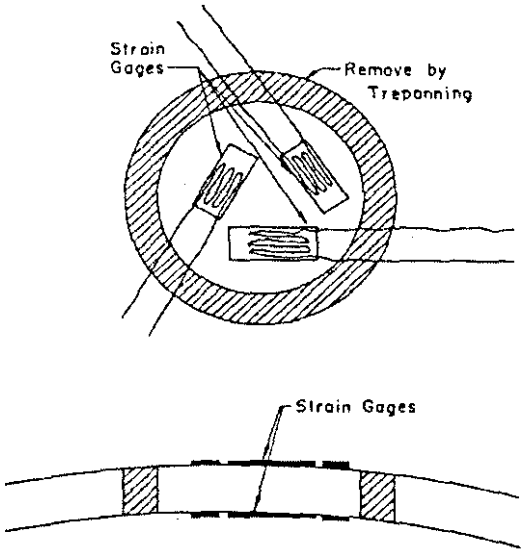

Fig1 : Complete stress relaxation technique

Applications: For all - round use, the measuring surface can be placed in any position. Advantages: Is a reliable method. Principle involved is simple; is highly accurate.

Disadvantages: Is a destructive method. Only gives the average stress for the area of the specimen from which the piece was removed, and does not measure locally concentrated stresses. The machining involved is sometimes expensive and time consuming [37].

2. The Mathar-Soete Drilling Technique

When a small circular hole is drilled in a plate containing residual stresses, residual stresses in areas outside the hole are partially relaxed. It is possible to determine residual stresses that existed in the area by measuring stress was proposed and used by Mathar and was further developed by Soete.

Summary of test method

1. A strain gauge rosette with three elements of the general type schematically illustrated in Fig. 2 is placed in the area under consideration.

2. A hole is drilled at the geometric centre of the strain gauge rosette to a depth of about 0.4 of the mean diameter of the gauge circle, D. The residual stresses in the area surrounding the drilled hole relax. The relieved strains are measured with a suitable strain-recording instrument. Within the close vicinity of the hole, the relief is nearly complete when the depth of the drilled hole approaches 0.4 of the mean diameter of the strain gauge circle, D.

3. Typical surface strain relieved when a hole is drilled is related to the relieved principal stresses by the following relationship:

$$\varepsilon_r = \left(\bar{\bar{A}} + \bar{\bar{B}} \cos 2\beta \right) \sigma_{\max} + \left(\bar{\bar{A}} - \bar{\bar{B}} \cos 2\beta \right) \sigma_{\min}$$

where εr = Relieved strain measured by a radially aligned strain gauge centered at P

A, B = Calibration constants

$\Sigma_{\max}$ = Maximum (most tensile) and

$\sigma_{\min}$ = Minimum (most compressive) principal stresses present at the hole location before drilling

β = angle measured clockwise from the direction of gauge l to the direction of σ_{max} the following equations may be used to evaluate the constants A and B

$$\bar{\bar{A}} = -\frac{\bar{a}}{2E}(1+\nu)$$

$$\bar{\bar{B}} = -\frac{\bar{b}}{2E}$$

where E = Young's modulus,

ν=Poisson's ratioand a & b are dimensionless, almost material independent constants.

Since any residual stress created by the selected drilling method will adversely affect the accuracy of results, a verification of the selected process is recommended when no prior experience is available. Such verification consists of applying a stain gauge rosette, identical to the rosette used in the test, to a stress free specimen of the same nominal composition and then drilling hole. If the drilling method is satisfactory, the stresses produced by drilling will be small [38].

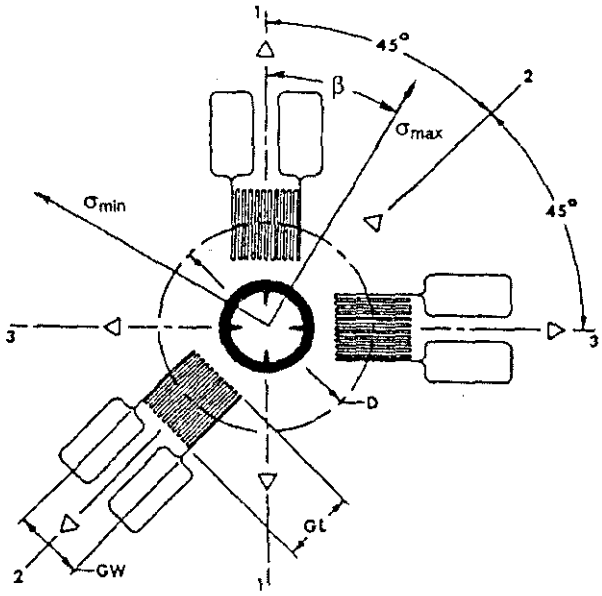

Fig 2: Schematic diagram showing the geometry clockwise strain gauge rosette for the hole of a typical three element drilling.

1.3.8 Procedure for computation Stresses

A specimen whose thickness is at least 1.2D is considered to be "thick". For such a specimen, to obtain eight sets of strain readings εl, ε2andε3, as the hole depth is increased in increments of 0.05D, up to final hole depth of 0.4D.

Specimen whose thickness is less than 0.4D is considered to be "thin". For such specimen, obtain one set of strain readings εl, ε2andε3, after a hole has been drilled through the entire thickness of the specimen.

The intermediate case when specimen thickness is between 0.4D and 1.2D is not within the scope of this Standard Test Method.

Compute the following combination stains for each set of measured strains εl, ε2 and ε3.

$$p=\frac{(\varepsilon_3+\varepsilon_1)}{2}$$

$$q=\frac{(\varepsilon_3-\varepsilon_1)}{2}$$

$$t=\frac{\varepsilon_3+\varepsilon_1-2\varepsilon_2}{2}$$

When working with a thick specimen, a test should be made to check that the residual stresses are uniform with the depth. In this case identify the numerically larger of combination strains q or t. Express each set of combination strains p and larger of q and as a percentage of their values when the hole depth=0.4D [38].

1.3.9 Computation of stresses:

a) Thin specimen

1. In the case of a "thin" specimen, only a single set of εl, ε2andε3 measurements is needed to calculate the magnitude and directions of the principal residual stresses. These stresses are assumed to be uniform through the specimen thickness.

2. The more tensile (or less compressive) principal stress σmax is located at an angle β measured clockwise from the direction of gauge 1 in Fig 10 similarly, the less tensile (more compressive) principal stress σmin is located at an angle β measured clockwise from the direction of gauge 3.

3 Compute the angle β from

$$\beta = \frac{1}{2}\tan^{-}\left(\frac{t}{q}\right)$$

a positive value of β , say β = 30° , indicates that σmax lies clockwise of the direction of gauge l. A negative value of β indicates σmin that lies 30 counterclockwise of the direction of gauge 1.

4. Compute the stresses σ_{max} and σ_{min} from

$$\sigma_{\max}, \sigma_{\min} = -\left[\frac{p}{\bar{a}(1+\nu)}\sqrt{\frac{\left(q^2+t^2\right)}{b}}\right]E$$

Use table2 to determine the numerical value

b) Thick specimen

In the case of a "thick" specimen, all sets of εl, ε2, ε3 measurements are used to calculate the magnitude and direction of the principal residual stresses. These stresses are assumed to be uniform throughout the hole depth.lues of the calibration constants corresponding to the hole diameter and type of rosette used [38].

Table 2: Numerical values of coefficients $\bar{a}$ and $\bar{b}$

Rosette A	$\bar{a}$					$\bar{b}$				
Blind hole	Hole Diameter, D_o/D					Hole Diameter, D_o/D				
Depth/D	0.30	0.35	0.40	0.45	0.50	0.30	0.35	0.40	0.45	0.50
0.00	.000	.000	.000	.000	.000	.000	.000	.000	.000	.000
0.05	.027	.037	.049	.063	.080	.051	.069	.090	.113	.140
0.10	.059	.081	.108	.138	.176	.118	.159	.206	.255	.317
0.15	.085	.115	.151	.192	.238	.180	.239	.305	.375	.453
0.20	.101	.137	.177	.223	.273	.227	.299	.377	.459	.545
0.25	.110	.147	.190	.238	.288	.259	.339	.425	.513	.603
0.30	.113	.151	.195	.243	.293	.279	.364	.454	.548	.638
0.35	.113	.151	.195	.242	.292	.292	.379	.472	.566	.657
0.40	.111	.149	.192	.239	.289	.297	.387	.482	.576	.668
Through Hole	.090	.122	.160	.203	.249	.288	.377	.470	.562	.651
Rosette B	$\bar{a}$					$\bar{b}$				
Blind Hole	Hole Diameter, D_o/D					Hole Diameter, D_o/D				
Depth/D	0.30	0.35	0.40	0.45	0.50	0.30	0.35	0.40	0.45	0.50
0.00	.000	.000	.000	.000	.000	.000	.000	.000	.000	.000
0.05	.029	.039	.053	.068	.088	.058	.078	.102	.127	.157
0.10	.063	.087	.116	.148	.189	.134	.179	.231	.286	.355
0.15	.090	.123	.162	.205	.254	.203	.269	.343	.419	.504
0.20	.107	.145	.189	.236	.289	.256	.336	.423	.511	.605
0.25	.116	.156	.202	.251	.305	.292	.381	.476	.571	.668
0.30	.120	.160	.206	.256	.309	.315	.410	.509	.609	.707
0.35	.120	.160	.206	.256	.308	.330	.427	.529	.631	.730
0.40	.118	.158	.203	.253	.305	.337	.437	.541	.644	.743
Through Hole	.096	.131	.171	.216	.265	.329	.428	.531	.630	.725
Rosette C	$\bar{a}$					$\bar{b}$				
Blind Hole	Hole Diameter, D_o/D					Hole Diameter, D_o/D				
Depth/D	0.40	0.45	0.50	0.55	0.60	0.40	0.45	0.50	0.55	0.60
0.00	.000	.000	.000	.000	.000	.000	.000	.000	.000	.000
0.05	.065	.084	.108	.130	.157	.105	.132	.158	.185	.217
0.10	.147	.191	.238	.293	.361	.250	.314	.373	.440	.519
0.15	.218	.281	.347	.420	.506	.391	.484	.570	.658	.754
0.20	.270	.343	.421	.504	.595	.506	.617	.719	.818	.912
0.25	.302	.381	.465	.554	.648	.591	.712	.823	.923	1.015
0.30	.321	.403	.491	.583	.679	.650	.778	.893	.994	1.081
0.35	.331	.415	.505	.599	.698	.690	.822	.939	1.041	1.125
0.40	.336	.421	.512	.608	.709	.719	.851	.970	1.073	1.154
Through Hole	.316	.399	.494	.597	.707	.623	.723	.799	.847	.859

1.For each of the hole depths corresponding to the eight sets of, εl, ε2, ε3 measurements, use Table to determine the numerical values of the calibration constants ā and b corresponding to the hole diameter and type of rosette used.

2. Compute the three combination stresses P, Q, and T corresponding to the three combination strains p, q and t using the following formula [38]

$$P = -E\frac{\left(\sum \bar{a}.p\right)}{\sum \bar{a}^{2}\left(1+\nu\right)}$$

$$Q = -E\frac{\left(\sum \bar{b}.q\right)}{\sum \bar{b}^{2}}$$

$$T = -E\frac{\left(\sum \bar{b}.t\right)}{\sum \bar{b}^{2}}$$

Where $\sum$ indicates a summation of the indicated quantities for the eight hole depths.

3. Computing the angle β from.

$$\beta = \frac{1}{2}\tan^{-}\left(\frac{-T}{-Q}\right)$$

4. Compute the stresses σmax and σmin from

$$\sigma_{\max}, \sigma_{\min} = P \pm \left(\sqrt{\left(Q^{2} + T^{2}\right)}\right)$$

(b) Measurement of Residual Stresses by X-Ray Diffraction

When external or internal forces are applied to a structure made up of crystals, the crystalline lattice is distorted, thus changing the inter-atomic distances. When the deformations exceed the elastic limit, plastic deformation takes place as a result of slip along the lattice planes. In any event, the change in the inter-atomic spacing is directly proportional to the stress.

Suppose that a monochromatic plane wave is introduced to the atomic planes in the direction AB, as shown in Fig.3 The reflected beams from successive parallel planes of atoms are reinforced in one direction, BC, The diffraction direction. Bragg's law defines the condition for diffraction as follows,

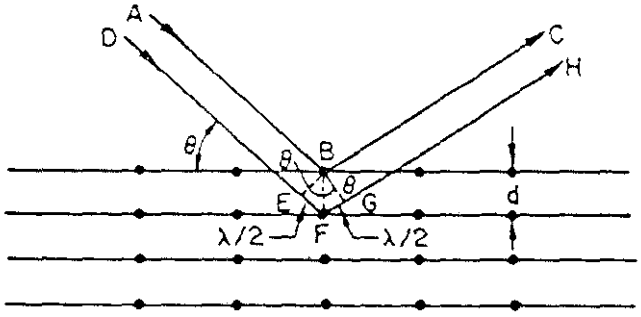

Fig.3: Diffraction produced by reflections from adjacent atomic planes of monochromatic plane wave [36].

$n\lambda = 2d\sin\theta$Where

λ = The wave length of incident beam,

θ = The angle between incident or reflected beams and surface of

reflecting planes.

d = The inter planar spacing

n = The order of reflection (n =1, 2, 3.....)

from above equation, if the wavelength of the x-ray is known, the inter planar spacing; d, can be determined by measuring the angle θ .

Fig.4 shows schematic diagram of setups of x-ray diffraction techniques. Two general techniques are employed in the recording of diffraction pattern; (1). The photographic or x-ray film technique, as shown in Fig 4 (a) and (2) The x-ray diffractometer or counter tube technique, as shown in Fig .4(b).

Fig.4 (a) shows a portable setup, which employs the film technique. The apparatus consists essentially of a film in a light tight cassette mounted perpendicularly to the incoming x-ray beam. The beam is collimated by the pinhole system inserted through a hole in the film. The film records the rays diffracted by the specimen, and shows, on development, near-circular rings. The diameter of a diffraction ring divided by the distance from the film to the specimen gives 2 tan (180-20) from which 0 is obtained for insertion in the above equation.

Fig.4 (b) shows an x-ray diffractometer setup. In most cases, the x-ray diffraction method differs only in the detector and the angle made by the specimen with the x-ray beam. The angle between the x-ray beam and the specimen surface is 90 degrees in the film method, but it is angle θ degrees for the diffraction method. A counter and a receiving slit are moved along a goniometric circle to record the intensity of the reflected beam. The diffraction angle is determined as the angle of maximum intensity.

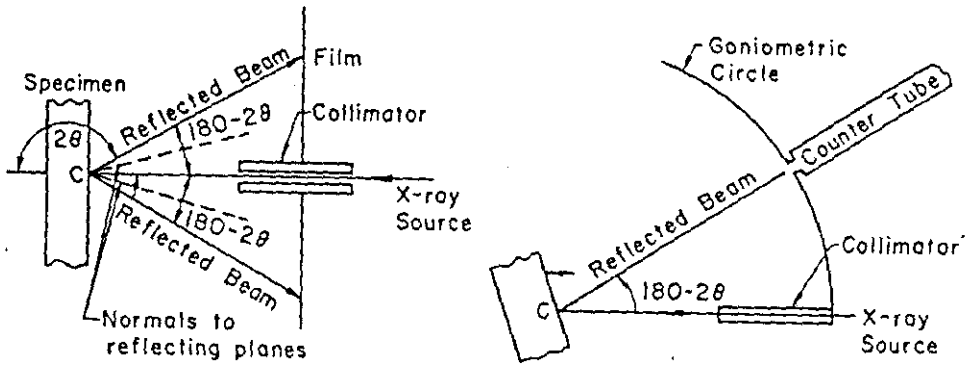

a) Portable X ray film technique b) X ray diffraction technique

Fig.4 : Schematic diagram of setup for X ray diffraction technique

The x-ray diffraction technique usually provides more accurate result than does the film technique. However, the size of the specimen that could be tested is limited by the geometry of the instrument [39].

c) Neutron Diffraction Technique

Neutrons can be used to measure stresses in the interior of components because of their relatively high penetrability in most engineering materials. The determination of residual stresses using neutron diffraction involves the measurement of interplanar spacing and, thus, in effect, the use of lattice planes as internal strain gages. If do is the stress-free interplanar spacing of interest, typically, one might measure the corresponding spacings, di (i= 1 and 3), along three mutually orthogonal directions (i) and then estimate the lattice strain(εi) according to equation,

$$\varepsilon i = (di - do)/ d0$$

The problem is, thus, reduced to one requiring the determination of the re.sidual stress state from the lattice strains. If the orthogonal directions are chosen appropriately, it is often sufficiently accurate to assume that these correspond to the principal axes, so that the stresses may be determined by equation from linear elastic theory to be

$$\sigma i = \{Ehkl/(1+\nu hkl)\}\ \varepsilon i + [\nu hkl\ Ehkl / \{(1+ \nu hkl)(1-2\ \nu hkl)\}]\Sigma 3j=1\ \varepsilon j$$

the stress in the direction i, and Ehkl and νhkl are the plane-specific Young's modules and poisson ratio, respectively. Good estimates of these are required if the residual stress field is to be determined accurately [40].

1.4 GAS TUNGESTEN WELDING

Tungsten inert gas (TIG) welding (Fig.5) is a widely used material joining process, especially for welding materials like stainless steel and non-ferrous lightweight metals such as aluminum, magnesium and titanium. A non-consumable tungsten electrode, shielded by an inert gas, is used to strike an electric arc with the base metal. The heat necessary to melt the base metal is provided by the electric arc. The quality of TIG welds ranks higher than that of any of the arc-welding processes, due to the reliability, clearance and strength of the weld.

In the experiments, TIG welding involves a number of process parameters. The quality of TIG welds is greatly dependent on the selection of process parameters such as welding current and welding speed, arc gap, inert gas flow rate.

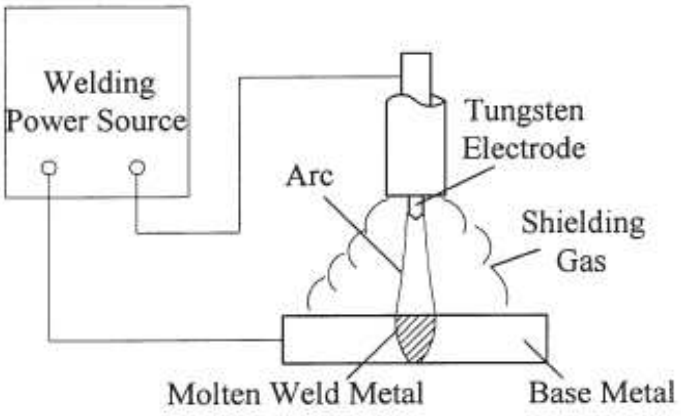

Fig.5: Process diagram of tungsten inert gas welding

The experiments were performed GTAW machine. The shielding gas used in the experiments was argon and the flow rate of argon was controlled by a flow meter. The base metals austenitic stainless steel(304) and medium carbon steel(508) plates and the thickness of the plates were 32 mm. As a consequence of the thick plates, multipass welding process was required.

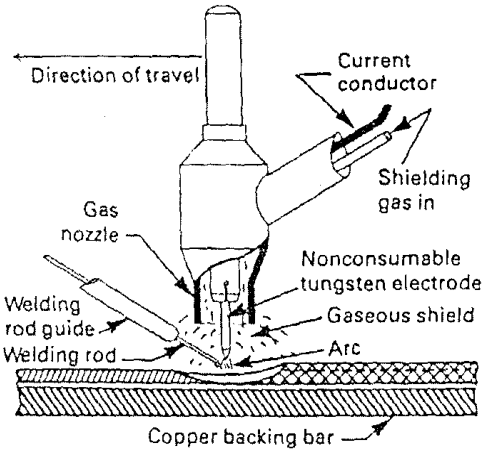

Fig.6: Gas tungsten arc welding

1.4.1 EQUIPMENT AND MATERIALS

The standard equipment for manual GTAW is quite simple and consists mainly of a power supply source, a welding torch, connecting cables and hoses for gas and water supplies. The accessories like feed wire mechanism, arc voltage control and feed-back system, electrode positioning device etc. are incorporated in the system when automatic and semiautomatic versions of the process are employed. The material used is tungsten rods and the major consumable are shielding gas were used [41].

1.4.2 POWER SOURCE

The power source is the heart of all the welding systems: reliability, accuracy and long life being the desirable characteristics governing the selection of a set. GTA welding system uses both D.C. and A.C. power sources with static volt-ampere (VI) characteristics of the drooping type that is, of the constant current type. In this type of power source, the slope of VI curve is relatively steep so that the change in arc length (arc voltage) will not create a major change in arc current. Thus, an inadvertent slight shift in the welder's hand will not have any discernable effect on the performance of the processes. That is why steeper the VI characteristic curve the more satisfactory the power source and that is particularly for manual GTA welding.

Fig: 7: Power source for TIG WELDING machine

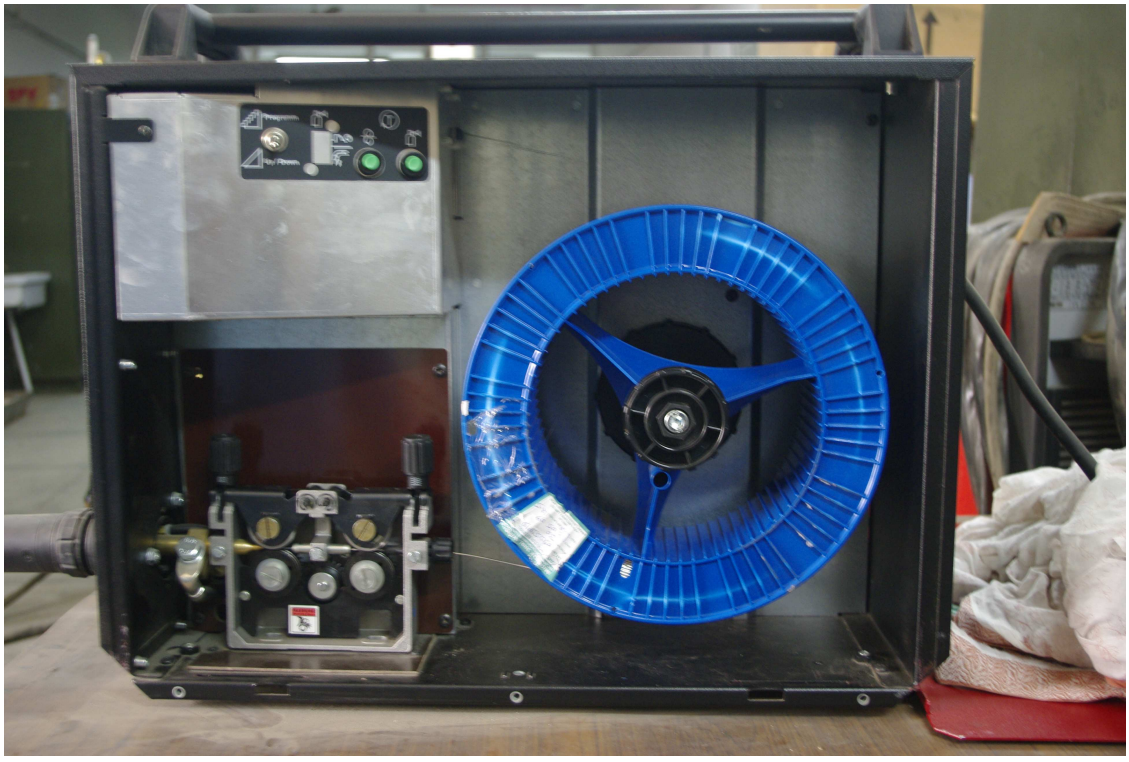

Fig 8: wire spool arrangements

Conventional shielded metal arc welding D.C. power source can be used for GTAW with the same rating but the A.C. power sources are derated usually to the extent of 25% to compensate for the current rectification inherent in the use of such power supply sources GTAW. The most used power

source for GTAW is the transformer cum rectifier unit with build-in water flow circuits and gas timers, which are turned on and off with control switch located on GTAW torch. A typical GTAW power source may operate with a range of 3 to 200 A or 5 to 300 A with a voltage range of 10 to 35 volts [41].

1.4.3 GTAW Torch

GTAW torches are designed for manual or automatic operation. Torches used for manual welding are provided with handles while those for automatic operation are without handles. There are two basic types of GTAW torches, the air cooled and the water cooled. The air cooled torch are used with current up to 150 A while the water cooled torches are used with currents up to 1000A. In this experiment water cooled torches are used.[41]

A collet is used to hold the electrode in a GTAW torch.The collet size varies according to the electrode size so as to ensure proper and adequate contact for clamping the tungsten electrode. The gas nozzle of a GTAW torch is its weakest part and is fastened to the torch body by threaded connection. These nozzles are generally made of ceramic material; however for low current torches metal nozzles can also be used. Specially designed gas nozzles are also available which reduce the gas turbulence to the minimum. With such a torch a nozzle to plate distance of up to 25 mm can be maintained.

1.4.4 ELECTORDE

Tungsten with melting point of 3410° C is used as the electrode material for GTAW and it provides the desired properties of high melting point low electrical resistance, good thermal conductivity and has the ability to emit electrons easily. These electrodes are classified into 4 types as listed in table 3.

Pure tungsten electrode (99.5%pure) is less costly and is used generally on less critical jobs than the thoriated and zirconated tungsten electrodes. A pure tungsten electrode has lower current carrying capacity with a.c. and is rather more prone to contamintation

Compared with pure tungsten electrodes thoriated tungsten electrodes have higher current carrying capacity, better electron emissivity, longer life and greater resistance to contamination. Easy arc imitation and better arc stability are also associated with these electrodes.

Table3: Classification of electrodes

AWS classification	Material	Thoria %	zirconia %	Tip color
EWP	Pure tungsten	-	-	Green
EWTh-1	Tungsten thorium	0.8-1.2	-	Yellow
EWTh-2	Tungsten n +2% thourum	1.7 – 2.2	-	Red
EWZr	Tungsten zirconium		0.15-0.40	Brown

Zirconated electrodes have properties that generally fall between those of pure and thoriated tungsten .however, these electrodes often show better performance with a.c welding by combining the easy arc imitation of thoriated tungsten electrode and the desirable arc stability or pure tungsten electrodes.

Too much current or an electrode too small in diameter will cause excessive tungsten erosion and may lead to tungsten inclusion in weld metal. If the current is too low or the tungsten electrode is too large in diameter, the arc will wander erratically over the tip of the electrode [41].

The choice of an electrode classification, size and welding current are influenced by the type and thickness of base metals being welded. The current carrying capacity of all types of tungsten electrodes are affected by the type of welding torch, the type of power source, the electrode extension beyond the collet, and the shielding gas, along with gas cup diameters recommended for use with different types of welding power sources [42].

In an arc, approximately 70% of heat is generated at the anode and 30% heat at the cathode. When the electrode is negative, it can carry a much higher current without overheating than when the electrode positive. Direct current with the electrode positive requires a much larger diameter to support a given level of current because the tip is not cooled by the emission of electrons but is heated by their impact. In general, an electrode of a given diameter operating on DC electrode positive (DCCP or reverse polarity) would be expected to handle only 10% of the current possible as compare with the electrode being negative (DCEN or straight polarity). Therefore, much larger electrodes are required for DCEP [42] .

1.4.5 SHIELDING GAS

The shielding gas used in TIG welding can be argon, helium or a mixture of the two, Argon is usually a better choice because it is heavier than air and therefore tends to provide a better blanket over the weld.

Shielding gases have a primary role to protect the weld from surrounding atmospheric oxygen and nitrogen. At an adequate flow rate they displace these two gases from the weld zone.

The ability of shielding gas to perform the protective role will depend on its chemical composition, which has significant influence on arc initiation, arc stability, and plasma diameter and plasma temperature. The physical and chemical natural of the shielding gas also affects other arc and weld properties such as surface oxidation, undercutting, porosity ,slag inclusions ,fusion and joint penetration [43] a gas with low ionization potential will easily ionize to form plasma.

Argon

The most commonly used shielding gas is argon, which is heavier than air.it is monotonic gas with an atomic weight of 40. The density of argon is 1.7837 gm/l at standard temperature and pressure. The gas is available in various grades, including a “high purity grade,” refined to minimum purity of 99.998%.

Welding grade argon is satisfactory for most welding applications. It is a chemically inert, colorless, odorless , tasteless and non toxic gas. It is obtained from atmosphere by the separation of liquefied air.

The chief factor influencing the shielding effectiveness is the gas density. Argon is approximately 1.3 times as heavy as air and ten times heavier than helium. Argon after leaving the torch gas nozzle tends to form a blanket over the weld area.

Although argon itself is chemically inert, it is readily ionized to form plasma. Impurities such as moisture and oxygen can cause unfavorable arc behavior and reduction in weld properties.

The reduced penetration of an argon shielded arc is particularly helpful when manual welding thin material, because the tendency for excessive melt-through is lessened the reduced penetration characteristic is advantageous in vertical or overhead welding since the tendency of the base metal to slag or run is decreased [43].

Argon is used more extensively than helium because of the following advantages

Easier arc initiation

Better control of the pool

Smoother, quicker arc action

Lower cost and great availability

Better cross-draft resistance due to higher density

Lower flow rate

Cleaning action when welding materials as aluminum and magnesium

with AC or DCEP

Reduced penetration

Helium

Helium is one of the lightest monatomic gases approximately ten times lighter than argon. It has an atomic weight of four .The density of helium is approximately 0.1785 gm/l .Helium is more expensive than argon. The gas is available in welding grade of approximately 99.95% purity, or high purity grade of 99.995% for most applications. Welding grade helium is satisfactory. Helium is chemically inert, colorless, odorless and tasteless gas.

Helium because of lighter than air tends to rise around the gas nozzle. Experimental works have consistently shown that to produce equivalent shielding effectiveness the flow of helium must be two or three times that of argon,. The same general relationship is true for mixtures of argon and helium, and particularly those high in helium content.

Helium transfers more heat into the work than argon. Since the arc formed in helium is considerably hotter than with argon, and because it has a higher conductivity, it can often promote higher welding speeds and improve the weld bead penetration profile [21].

Higher welding speeds are possible with helium because arc voltage can be obtained at the same current .Since the arc voltage in helium is higher, a lower current is possible to get the same arc power hence, welds can be made at higher speeds in as much as the increase in power comes from the increase in voltage rather than in current [43].

Argon and Helium

Helium–Argon mixtures are used to take advantages of the optimum operating characteristics of each gas, the superior arc initiation and stable arc characteristics of argon and higher thermal conductivity of helium .These mixtures are used to increase the voltage and heat input of the arc while maintaining the favorable characteristics of argon. Helium rich mixtures are preferred in order to achieve the significant benefit from helium. The most common used mixtures contain 75% helium. helium addition less than 50% have little influence on the arc characteristics .The commonly used mixture of helium/argon is in the proportion of 75% and 25% .The speed and quality of AC welding of aluminum can be improved with this type of mixture with cleaning action as good as with pure argon to maintain the good arc behavior of argon and as well as to achieve the heat input characteristic of helium [43].

1.4.6 GAS FLOW RATES

The flow rate of argon should be adequate to obtain a clean weld. This depends on several factors such as type of parent metal, current used, shape and size of nozzle, type of joint and whether the work is done indoors or outdoors .Generally, a higher rate of flow is required with higher welding currents for outside corner joints. Sharp bends, sharp edges and massive volume changes in the gas supply system may cause turbulence in the gas flow and turbulence in gas flow system can cause instabilities in the welding arc. Flow rates of 5 to 15 liters /min, generally will suffice to weld thickness form 1 to 35mm.

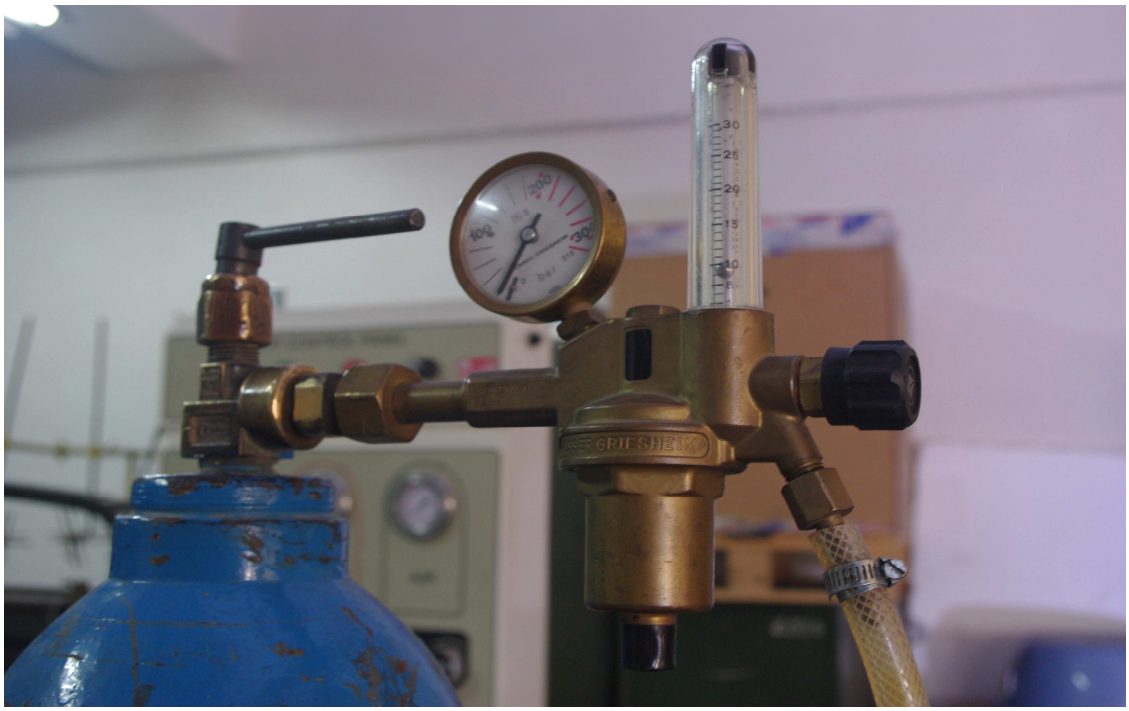

FIG 9: Shows the gas flow rate of shielding gas.

Fig 10 TIG welding process

1.4.7 OPERATION OF GTAW PROCESS

The main steps in successful operation GTAW include:

Electrode preparation

Installation of backup plate or purging

Initiation of arc

Maintenance of the Arc

Welding techniques

Stoping the Arc

1.5 QUALITATIVE EVALUATION

Historically, welding has replaced riveted construction in many engineering structures. It is now scarcely possible to design an industrial structure without a welded joint. Inability to use appropriate testing, measurement and control procedures correctly may lead to unexpected and unforeseen problems in welding. No weld is completely perfect. Welds may be compared to small castings except that weld metals cools rapidly due to heat sink provided by base metals. This results in thermal stresses which may lead to cracking and entrapment of gases or foreign materials within weld. These and other defects may cause premature failure of the weld during manufacture and/or service [44].

1.5.1 Defects associated with residual stresses

The two major causes of weld related failures in industrial structures are due to fatigue and stress corrosion cracking. Both these modes of failure depend to a large extent, on the presence of tensile residual stress on the surface of a component/structure. Hence residual stress is a very important factor and requires accurate assessment [45].

1.5.2 Testing, Measurement and Control of welds

The meaning and scope of TMC of weld is broadly understood by those associated with the design, fabrication and quality assurance practices. Testing of welds implies the use of both destructive and non-destructive techniques which together assess the quality of a weld joint in terms of the design specifications. Measurement of weld implies the measurement of various parameters associated with welding which affect the quality of a welded joint in terms of the design specification. These could be (a) pre-weld fitting paeameters like bevel angle, dimensions etc.,(b) welding parameters such as welding current, heat input etc. and (c) post-weld parameters like amount of delta ferrite as in the case of austenitic stainless steel weldments[45].

1.5.3 Non Destructive Testing

NDT plays an important role in reducing the chances of weld failure, both through its application during fabrication and through its use in service. The importance of the role of NDT in preventing weld failure varies depending on the particular application.

Probability of weld failure = (Probability of flaw occurring) X (Probability of NDT missing the flaw) X (Probability of the flaw growing)

Quality characteristics of welds having defects such as cracks, inclusions, porosity, lack of penetration, lack of fusion, lack of bond and undercut can be evaluated by NDT methods. Present range and capabilities of NDT techniques promise evaluation of weld joints for the most significant service conditions. Various NDT methods can be employed to evaluate a welded component depending upon the material, thickness, sensitivity requirement, accessibility for inspection etc [46].

1.5.4 Visual Inspection

Visual Inspection is probably the most widely used among the non-destructive tests. A simple visual inspection should be carried out first. A simple visual inspection can reveal gross surface defects thus leading to an immediate rejection of the component and consequently saving much time and money, which would otherwise be spent on more complicated means of testing. Visual inspection methods have developed to examine the weld joint for the presence of finer defects to a very high degree of precision. With the advent of CCD cameras, microprocessors and computers, visual examination can be carried out very reliably and with minimum cost. Image processing, pattern recognition and automatic accept/reject choices are used when large number of components is to be assessed [47].

1.5.5 Liquid Penetrant Testing

Liquid Penetrant Testing is another NDT method to detect surface and sub surface open to surface in welded materials. This method can be used in root passes and subsequent passes to detects and repair the defects in the weld. Following is the testing procedure and the sequence employed:

(a)Liquid penetrant is applied to the surface of the product for a certain predetermined time

(b) Penetrant seeps through the defects by capillary action

(c) Excess penetrant is removed

(d) Surface is dried and developer is applied

(e) Penetrant remained in the defect is absorbed by the developer

(f) Presence, location, size and nature of defect is revealed

Care should be taken so that chemical constituents of the liquid penetrant and developer should not affect the material [47].

1.5.6 Magnetic Particle Testing

This method is based on the principle that when a ferromagnetic material under test is magnetized, discontinuities which lie in a direction generally traverse to the magnetic field will cause the leakage field around the discontinuity. When finely divided ferromagnetic powder is sprinkled over the surface, some of these particles are gathered and held by the leakage field. This magnetically held collection of particles from an outline of the discontinuity indicates its location, shape and extent.

Procedure:

(a) Material is magnetized

(b) Defects which lie in a direction traverse to the field cause leakage field around them

(c) Ferromagnetic powder is sprinkled over the surface

(d) Particles gather and are held by the leakage field

(e) Outline of the discontinuity is formed indicating its location, shape and extent

(f) Component demagnetized.

To get the highest sensitivity, fluorescent magnetic particles suspended in oil using full wave DC continuous technique is employed[47].

1.5.7 Ultrasonic Testing

Ultrasonic Testing is a NDT method in which sound waves of high frequency are introducedinto the material being inspected to detect internal flaws and to study the properties of the material. The sound waves travel into the material with some loss of energy due to attenuation and are reflected at interfaces. In most of the applications, the reflected beam is detected and analysed to define the presence and location of defects and for quantitative evaluation.

Defects like cracks, shrinkage cavities, lack of fusion pores and bonding faults which act like metal-gas interfaces can be easily detected by this method. Inclusion and other inhomogeneities in the metal can also be detected due to partial reflection or scattering of the ultrasonic waves.

Ultrasonic inspection is mostly carried out at frequencies between 1 and 25 MHz. The inspection system includes an electronic flaw detector having a sweep circuit, pulse generator, clock circuit and a cathode ray tube.A transducer (probe or search unit) having a piezoelectric crystal that emits a beam of ultrasonic waves when bursts of alternating voltages are applied to it.

A couplant to transfer energy of the ultrasonic waves to the test piece [47].

CHAPTER 2 LITERATURE REVIEW

Techniques for measurement of residual stress using successive extension of a slot are known in the technical literature by several names: crack compliance method, fracture mechanics approach, successive cracking method, slotting method, rectilinear groove method, etc. The term originally coined by Cheng and Finnie [48], the crack compliance method or compliance for short, is used as an inclusive term. The name came from the similarity of this technique to the compliance method for measuring crack length in a fatigue or fracture specimen [49]; a known load was applied to a cracked specimen, and the resulting strain was used to determine the crack length. In the residual-stress crack compliance method, the crack length is known and the measured strain is used to calculate the residual stress.

Schwaighofer's [50] early work (1964) deserves mention as the first use of a slot to measure residual stress. He machined two slots in a part and determined the surface residual stress using strain measurements taken between the slots. He recognized that the subsurface stress variation would affect the measurement but did not postulate the possibility of using successive slot extensions to measure the variation. The measurement of strain at incremental depths to measure a residual stress profile was introduced for hole drilling measurements by Soete and VanCrombrugge [51] and Kelsey [52], although their implementations were theoretically incorrect.

What is termed the crack compliance method was originally introduced by Vaidyanathan and Finnie in 1971 [52]. They measured residual stress in a butt-welded plate by introducing a hole in the plate and then extending a slot from the hole using a jeweler's saw. At each increment of slot length, they measured the stress intensity factor, KI, using a cumbersome photoelastic technique. Then they invented a solution for KI to get a closed form solution for residual stress from the variation of KI. The method appeared to successfully measure the residual stress, although there was little with which to compare the results.

This method saw minimal use in the following years. The experimental difficulty in performing the photoelasticity measurements likely discouraged others from applying Vaidyanathan and Finnie's idea. The original work also relied on a closed form solution for KI for a crack subjected to arbitrary loading on the crack faces. Such solutions were not available for many practical configurations.

By the mid 1980s, technological advances stimulated new research using the crack compliance method. This new research is evidenced by publications from researchers in several countries:

Cheng and Finnie [48] from the United States, Ritchie and Leggatt [55] from the Netherlands and the United Kingdom, Fett [54] from Germany, Reid [56] from the United Kingdom, and Kang, Song, and Earmme [57] from South Korea. Computational advances had made it both possible and relatively simple to solve the solid mechanics problems necessary for application of the compliance method for arbitrary geometries. These computational techniques also allowed the residual stresses to be calculated from measured strains or displacements, instead of from KI. This approach allowed the much more convenient and universally available strain gauges to replace photoelastic measurements. Since these early publications, the technique has seen many advances and new applications.

Special note should be made of the driving force behind the development of the crack compliance method, Professor Iain Finnie of the University of California, Berkeley. Although he never appears as the lead author, he invented the method [58], and has been instrumental in its development.

One might prefer to measure residual stress nondestructively. However, there are crucial gaps in the capabilities of nondestructive techniques [59]. The two primary nondestructive techniques are x-ray diffraction (XRD) and neutron diffraction (ND). XRD can nondestructively measure residual stress in crystalline materials to a maximum depth of about 0.05 mm. Measuring to a greater depth requires layer removal, such as by etching, and makes the measurements destructive. ND can measure residual stress to depths of many centimeters but is generally constrained to measuring a volume no smaller than a cube 1 to 2 mm on a side. This constraint makes it difficult or impossible to resolve residual stress variations over distances of less than about 1 mm. Furthermore, ND cannot measure stresses much deeper than about 50 mm for engineering materials. Therefore, considering ND and XRD, nondestructive measurement is not feasible over the large range from 0.05 mm to 1 mm and for depths greater than about 50 mm. Unfortunately, residual stresses that vary over this range are produced by many of the most common manufacturing processes: heat treating, machining, forging, cladding, and casting, for example. At the same time, the primary contribution of residual stress to mechanical failures, such as from fatigue and fracture, can occur over the 0.05 mm to 1 mm range. Additionally, there are other limitations to the XRD and ND methods:

(1) Sensitivity to grain size and texturing effects. Crystalline structural anisotropy may render the measured residual strains to be ambiguously related to the actual macroscopic residual stress.

(2) Complete inability to measure non-crystalline materials.

(3) Difficulty measuring stresses on curved surfaces for XRD. The path length of the scattered beam is increased, which cannot be distinguished from strain, leading to errors.

(4) A typical stress depth profile obtained using XRD or ND methods may take days to a week. The same stress profile using crack compliance could be accomplished in one day.

Previously, welding residual stress analysis used only experimental measurement methods. These methods can be divided into two categories. One is destructive method. For instance, Pang and Pukas [60] measured stresses by hole drilling and strain gauge techniques. The other is non-destructive method. For example, Chandra [61] and Brand [62] measured residual stresses in a weld bead by X-ray diffraction (XRD) techniques; Chu [63] measured welding residual stresses using supersonic waves. However, both categories of measurement methods only obtain incomplete stress distributions and are time-consuming. Furthermore, the XRD method is highly accurate, but is limited by the fact that only information is obtained about a relatively thin surface layer [64].

Speckle interferometry has been used for small deformation measurement for many years. In the 1970's and 80's, the technique was first adapted for measuring residual stress using the hole drilling method[65]. The obvious advantage was elimination of the strain gage, which reduced the time required for measurements, but the technique also expanded the range of surface textures and geometries available for measurement. The development of the electronic speckle pattern interferometer allows the data acquisition to be automated and integrated with computer analysis, further increasing the efficiency of the technique. The ability of this system to quickly perform multiple drillings at low incremental cost makes it an ideal tool to study the effects of hole drilling variables on the accuracy of the measurements.

L.M. Lobanov et.al[] In discussed the group of the currently available methods for experimental determination of the residual stresses in the structures, special attention has been given to the method of the probing hole, in which a continuous or blind hole is drilled at the investigated point on the surface of the object, and the strains caused by elastic unloading of the volume of the material during the release of residual stresses are measured in the vicinity of the hole. The stresses are measured using special strain gauges bonded in accordance with the specific procedure.

The values of these strains are subsequently used to calculate the main directions and appropriate values of the residual stresses, using calculation or analytical models. It was pointed out that number of difficulties associated with the application of the bonded strain gauges can be eliminated using laser interferometry methods.

Man gyunna et.al []fuzzy neural network model is presented to predict residual stress for dissimilar metal welding under various welding conditions. The fuzzy neural network model, which consists of a fuzzy inference system and a neuronal training system, is optimized by a

hybrid learning method that combines a genetic algorithm to optimize the membership function parameters and a least squares method to solve the consequent parameters. The data of finite element analysis are divided into four data groups, which are split according to two end-section constraints and two prediction paths. Four fuzzy neural network models were therefore applied to the numerical data obtained from the finite element analysis for the two end-section constraints and the two prediction paths. The fuzzy neural network models were trained with the aid of a data set prepared for training (training data), optimized by means of an optimization data set and verified by means of a test data set that was different (independent) from the training data and the optimization data. The accuracy of fuzzy neural network models is known to be
sufficiently accurate for use in an integrity evaluation by predicting the residual stress of dissimilar metal welding zones.

CHAPTER 3 PROBLEM FORMULATION

The Reactor Pressure Vessel steel (20 Mn-Mo-Ni 55) & Stainless Steel bimetallic weld joints are widely used in Nuclear Reactors. The use of bimetallic weld view. The joining of RPV steel & Stainless Steel should be done in such a way so as to reduce the Residual stresses produced during joining as these affect its failure. The joining of RPV steel-Stainless Steel is done by using buttering layer procedure. From the literature review it is conclude that the generation of residual stresses in bimetallic weld is a crucial safety issue and demands research focus to and understand the evolution of the residual stresses in bimetallic welds.

The present work identified this challenge and is an effort to evaluate the residual stresses developed in reactor pressure vessel Steel-Stainless Steel welds during TIG welding and to see the effect of TIG welding parameters in the generation of these stresses.

Thus the objective of this work was to make sound TIG welded Reactor Pressure Vessel Steel-Stainless Steel joints with suitable Tensile strength, Impact strength, Microstructure, Micro hardness & composition. An attempt to measure the Residual Stresses was to be made in this work and correlate it with temperature profile during the welding cycles.

CHAPTER 4 EXPERIMENTAL PROCEDURE

4.1 WELDING

Base materials used for welding were austenitic stainless steel and mild steel. There compositions are given in Table No.4 and 5.

Table 4: Chemical composition of austenitic stainless steel

C	Mn	Si	Ni	Cr	Fe
0.06	4.05	4.5	13.4	22.2	44.1

Table 5: Chemical composition of mild steel

C	Mn	Si	Al	Fe
0.19	1	0.29	0.02	Balance

Size of each plate was 150mmx75mmx32 mm. Four plates of stainless steel and four plates of mild steel were used to prepare four weld coupons. Plates were welded along their lengths.

4.1.1 Welding process:

Continuous TIG welding process was used to make welded joints. Joint design used was single U-butt joint shown in Fig.7. Buttering layer of variable thickness were laid on mild steel plates to prevent carbon migration. Thicknesses of buttering layer were 0mm, 4mm, 6mm, and 8mm. ER 309 was the material for buttering layer. Welds were made using ER 308 as filler wire. Diameter of filler wire was 1.6mm. Arc voltage was 18 Volts. Current for root passes and finishing passes was 150 Ampere and for intermediate passes was 180 Ampere. Welding was carried out as per Welding Procedure Specification (WPS). Polarity was DC, electrode negative.

Shielding gas used was commercially available Argon gas (99.97% pure). Gas flow rate of 10 lit/min was chosen because good welding characteristics were obtained at this rate.

Table 6: Chemical composition of filler wire ER309 used for buttering:

C	Mn	Si	Cr	Ni	S	Fe
.02	1.7	0.4	23.5	13.0	0.01	Balance

Table7: Chemical composition of filler wire ER308 used for welding:

C	Mn	Si	Cr	Ni	S	Fe
0.02	1.5	0.4	20.03	9.9	0.01	Balance

4.1.2 Welding Equipment:

Welding was carried out on CEBORA Article 349 welding machine which is a semi-automatic machine. Welding was done manually.

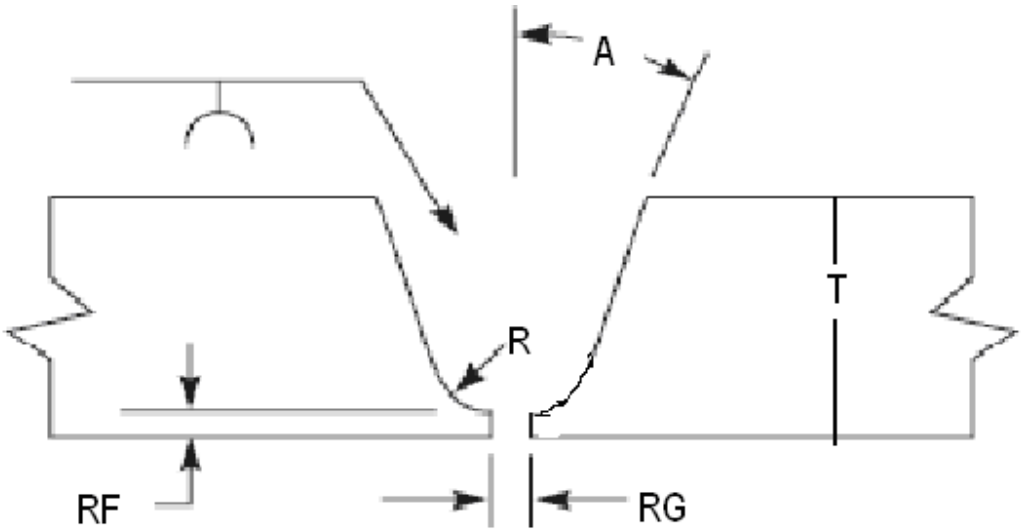

T = 32 mm
A = 22.5°
R = 4 mm
Root face = 2.4 mm
Root Gap = 1.6 mm
Fig.11: Groove Design

4.2 Temperature measurement

Temperature measurement was carried out using nickel and & nickel –chromium thermocouple. There thermocouples were used simultaneously. These thermocouples were fixed to the work piece. for measuring the temperature at the weld bottom of weld pool a hole with a diameter of 2 mm was drilled from the back surface of the test plate to place the thermocouples in proper location twin bore refractory tube was used . The temperature measurements at the surface were made at the weld toe. Thermocouple at this point was fixed with in a drilled hole of 1mm depth & 1.5 mm diameter .the material surrounding this hole was punched with a centre punch. Due to this the hole contracted and gripped the thermocouples. There were six thermocouples fixed to surface at 10 mm ,15mm & 20mm from the centre line in german steel and 10mm,15mm & 20 mm from the centre line in stainless steel. These thermocouples were connected to digital temperature measuring device which could produce the and temperature in the form of printed output v. this device could measure transient temperature of 20 points simultaneously. Following picture shows actual picture of the cross section of the work piece having thermocouples fixed in a drilled hole.

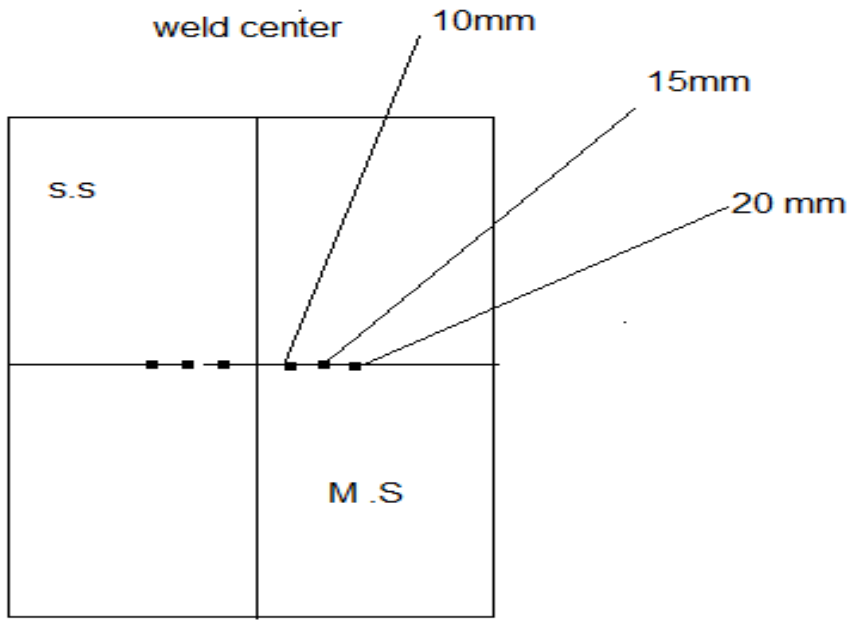

Fig 11.1: Mountings of thermocouples at different points

Fig 12 . Mountings of nickel& nickel chromium thermocouples in weld coupon

Fig 13: Arrangement of recording of temperature in bimetallic weld

4.3 RESIDUAL STRESS MEASUREMENT

Hole drilling technique was used for the measurement of residual stresses in weld coupons; in this technique, strain gauges were mounted in the specimens. The portion of the specimen containing the gauge is made stress 'free by drilling a hole· at the center gauge system and change I strain is measured by data logger. From the measured strains principal stresses were calculated according to ASTM-E-837-01 standard. A brief description of this method has already been given in Chapter 2.

Three element strain gauge rosettes were used for the stress measurement. Different rosettes were used for stainless steel and mild steel portions. Specifications of these rosettes are following:

Specifications of strain gauge rosette used for austenitic stainless steel

Trade name : FRS-2-17

Company name : TML, Japan

Gauge length : 1.5mm

Gauge resistance : 120 ± 0.5 'H

Gauge factor : 2.07

Gauge circle diameter: 6mm

Transverse sensitivity: 0.6%

Coefficient of thermal expansion: 16.2 x 10E-6 /°C

Tolerance : ± 0.85 [(urn/m) /°C]

Specifications of the strain gauge rosette used for mild steel

Trade name : FRS-2-11

Company name : TML, Japan

Gauge length : 1.5mm

Gauge resistance : 120 ± 0.5 n

Gauge factor : 2.07

Gauge circle diameter: 6mm

Transverse sensitivity: 0.6%

Coefficient of thermal expansion: 11.8 x 10E-6 /°C

Tolerance . : ± 0.85 [(um/m) /°C]

4.3.1 Mounting of strain gauges

Residual stress was measured by locating strain gauge rosettes at various locations of the weld coupon. Each rosette was mounted at mild steel base, mild steel HAZ, stainless steel HAZ stainless steel base portion. All coupons have four measurement points.

Fig 14:Mounting of strain gauge in weld coupon

The surface of the test plate where gauges are mounted was properly cleaned with acetone.

4.3.2 Drilling Operation

Drilling operation was performed with portable drilling machine with the speed range of250-530 rpm. The diameter of the drilled hole was 1.8mm. The hole was drilled at the center of the rosette up to *OAD* i.e. 2.6mm depth, where D is the gauge circle diameter along the thickness of the test plate.

4.3.3 Data Logger

The data taker range of data logger is microprocessor based battery powered or mains powered data loggers which can measure all of the fundamental signal types and have direct support built in for a wide range of commonly used sensors.

Data manipulation includes sensor calibrations, real time statistical functions and real

time calculations, The acquired data can either be returned to a host computer in real time or can be logged into memory for later recovery. Data can be stored in battery backed internal memory card which can be periodically removed from the logger to transport the data. Specifications of the data logger are as follows:

Model DT500

Company Data Taker Pty Ltd.

Common mode range- ± 3.5V

Digital channels Input/ Output - 4/4

Range -10^4 to 10^4 ppm

4.3.4 Recording the strain

The values of the released strain were recorded in a data logger. Prior to the drilling, values of strain at the measuring points were calibrated to zero in each trial. Data logger gives values in ppm which converted into micro strain.

Table 8 .Measured strains in weld coupon 1

points	Strain (μm)	Strain (μm)	Strain (μm)
1	-1469	-2707.44	-3806.76
2	-1463.42	-1467.54	-1469.04
3	6020.155	-501.565	1819.71
4	5146.087	-1155.88	758.4348

Fig 15: Show the drilling operation during the stress relaxation techniques

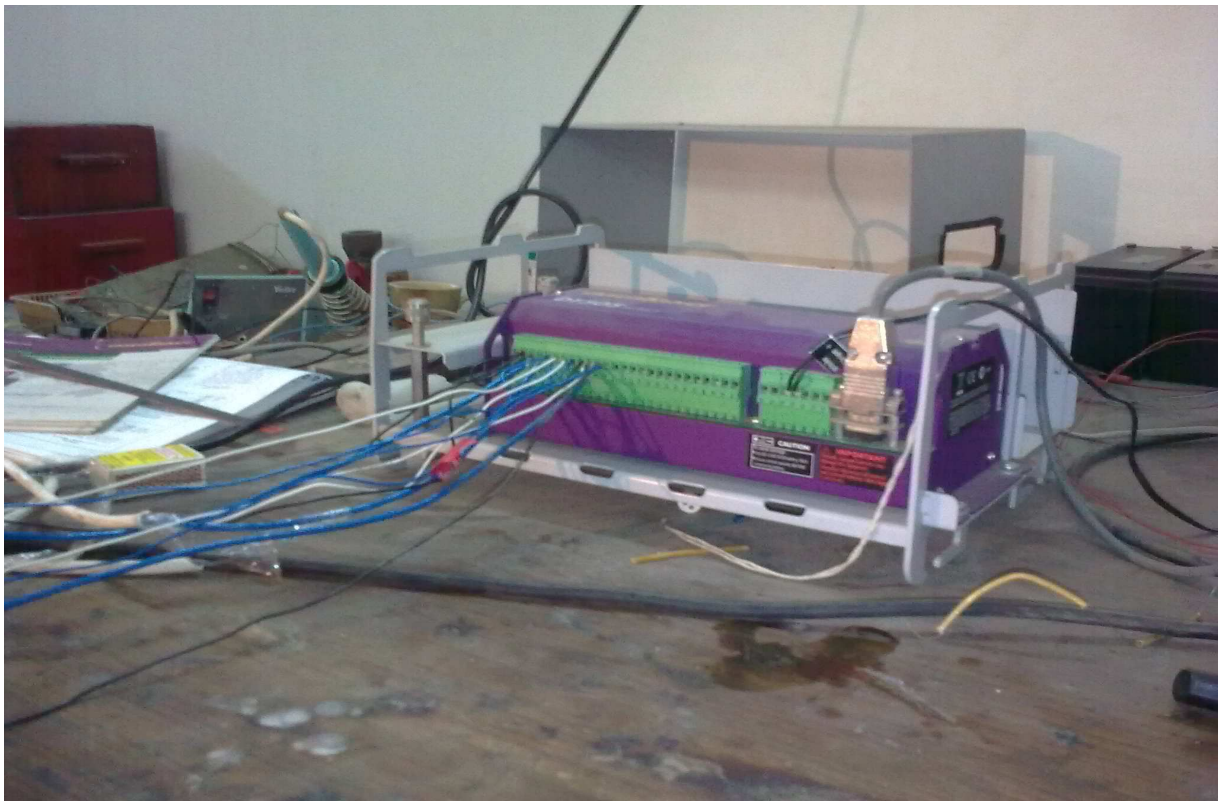

Fig 16. Show the data taker recording the strain

4.3.5 Residual stress calculation

Calculation of residual stress was done as follows;

Three gauges of the rosette measured the following ppm values in SS HAZ in weld coupon with 8mm buttering layer:

Gauge 1 = -757.69 ppm

Gauge 2 = -758.35 ppm

Gauge 3 =-785.35 ppm

Micro strains are calculated by the following relationship

Micro strain = (ppm x 4)/ gauge factor

Micro strains calculated are

Gauge 1 = -1464.14 ppm

Gauge 2 =-1465.41 ppm

Gauge 3 =- 1517.58 ppm

$\overline{A}$, $\overline{B}$ = Calibration constants which are given as and can be calculated using the relation

$\overline{A} = -\overline{a} / 2E(1+\nu)$

$\overline{B} = -\overline{b} / 2E$

where v = 0.29

E=193MPa

$\overline{a}$ =0.118

$\overline{b}$ =0.329

Putting above values in the equations

$\overline{A} = -\overline{a} / 2E(1+\nu)$ = -3.88x10^-13

$\overline{B} = -\overline{b} / 2E$ =-8.52*10^-13

Now principal stresses are calculated using the following equation.

$\sigma 1,2 = (\varepsilon 1 + \varepsilon 2 / 4 \times \overline{A}) \pm \sqrt{2} / 4 \times \overline{B} \sqrt{(\varepsilon 1 - \varepsilon 2)^2 + (\varepsilon 2 - \varepsilon 3)^2}$

From the above relation $\sigma 1$ =186.5021 MPa and $\sigma 2$ =190 Mpa

Angle β was computed using the relation

$$\tan 2\beta = \frac{\varepsilon_3 - 2\varepsilon_2 + \varepsilon_1}{\varepsilon_3 - \varepsilon_1}$$

Longitudinal (σL and transverse (σT) residual stresses are calculated from the following relationship.

$\sigma L = \sigma 1 \cos \beta + \sigma 2 \sin \beta$

$\sigma T = \sigma 2 \cos \beta - \sigma 1 \sin \beta$

Longitudinal residual stress σL = 18.06896 MPa

Transverse residual stress σT = 265.8792MPa

Longitudinal residual stress and Transverse residual stress at other points were calculated following the above procedure.

4.4 TENSILE TESTING

Tensile test were carried out as per ASTM E 602 using smooth bar tensile test specimens having dimensions. Before starting the test the diameter of each specimen was measured and gage length of 60mm for weld metal & base metal. Specimen was fixed firmly into the jaws of the machine. Load was applied and increased gradually till fracture occurred.

4.5 MICRO HARDNESS

Weld specimen prepared for micro hardness containing all zones such as base metal, weld metal , interface & HAZ.Hardness are measured across the weld joints in every zone is taken at constant load of 1000 gm and loading time of 20 sec.microhardness is taken in vicker hardness

CHAPTER 5 RESULTS & DISCUSSION

5.1 MACROSCOPIC BEHAVIOUR

Result of experiment performed are discussed in this chapter which includes temperature measure measurement at various points in weld coupons, tensile test,impact toughness measurement and chemical compostion.

5.1.1 TEMPERATURE MEASUREMENT

There were six thermocouples fixed to surface at 10 mm ,15mm & 20mm from the centre line in german steel and 10mm,15mm & 20 mm from the centre line in stainless steel. These thermocouples were connected to digital temperature measuring device connected to data acquisition system which could produce the temperature in the form of printed output the shown in table 9. This data acquisition system could measure transient temperature of 20 points simultaneously. The following graphs 17-19

Table 9: Measurement of temperatures in weld coupon 1

Time in sec	Temp in ℃	Temp in ℃	Temp in ℃	Temp in ℃	Temp in ℃	Temp in ℃
2	863.07637	807.62233	725.49082	830.67876	770.72217	667.46905
50	856.76816	801.53443	722.95682	826.48192	768.86118	666.0654
100	848.28562	793.82137	718.41887	819.34874	767.36374	664.61287
400	810.16594	757.69132	678.8792	780.72232	734.76338	650.0484
800	767.408	716.12638	639.6065	738.2233	700.5623	615.897
1000	746.95363	696.95363	618.68069	718.20456	680.81417	607.897
1200	732.86303	682.24299	608.05444	708.1494	660.77262	578.86354
1600	703.91501	654.05725	582.25655	680.28654	650.93069	550.78
2000	681.91408	632.24256	565.14976	661.66793	630.60521	529.05439
2400	663.79138	614.02357	549.40704	646.78191	626.78317	515.60427
3000	642.14117	592.69255	531.26993	627.14754	622.7735	511.73235

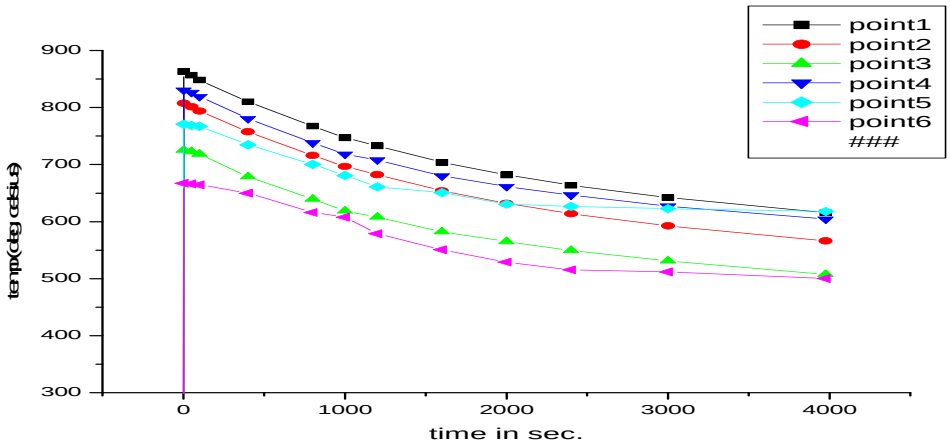

Fig 17: Temperature profile for coupon 1 at various points of measurement

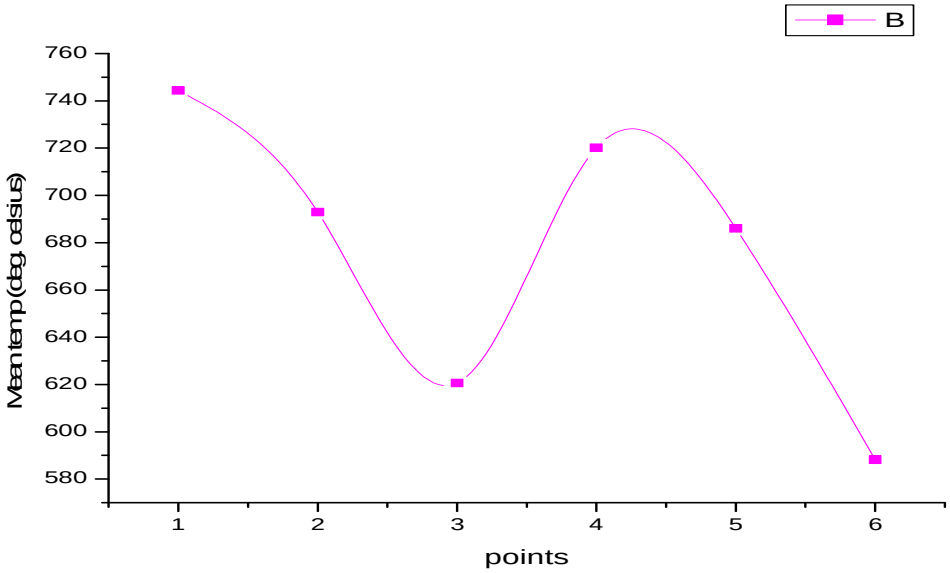

Fig 18: Mean temperature profile for coupon 1 at different points

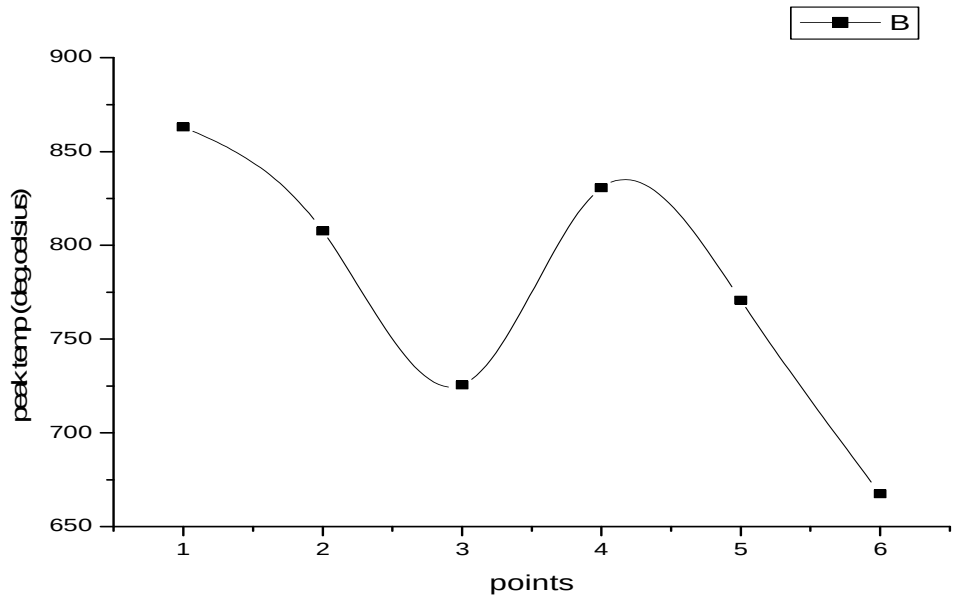

Fig 19: Peak temperature profile for coupon 1

Table 10: Measurement of temperatures in weld coupon 2

Time in sec	Temp in℃ Point1	Temp in℃ Point2	Temp in℃ Point3	Temp in℃ Point4	Temp in℃ Point5	Temp in℃ Point6
50	858.0049	801.8796	724.1908	826.9379	669.0952	566.2964
100	849.5223	794.1666	719.6529	819.8047	667.5977	564.8439
400	811.4026	758.0365	680.1132	781.1783	657.9974	555.2794
800	768.6447	716.4716	640.8405	738.6793	648.2142	545.6646
1000	748.1903	697.2988	619.9147	718.6606	644.0482	541.8156
1200	734.0997	682.5882	609.2884	708.6054	641.0066	539.0945
1600	705.1517	654.4025	583.4906	680.7425	635.1647	533.1956
2000	683.1508	632.5878	566.3838	662.1239	630.8392	529.2854
2400	665.0281	614.3688	550.641	647.2379	627.0172	525.8353
3000	643.3779	593.0378	532.5039	627.6035	623.0075	521.9634

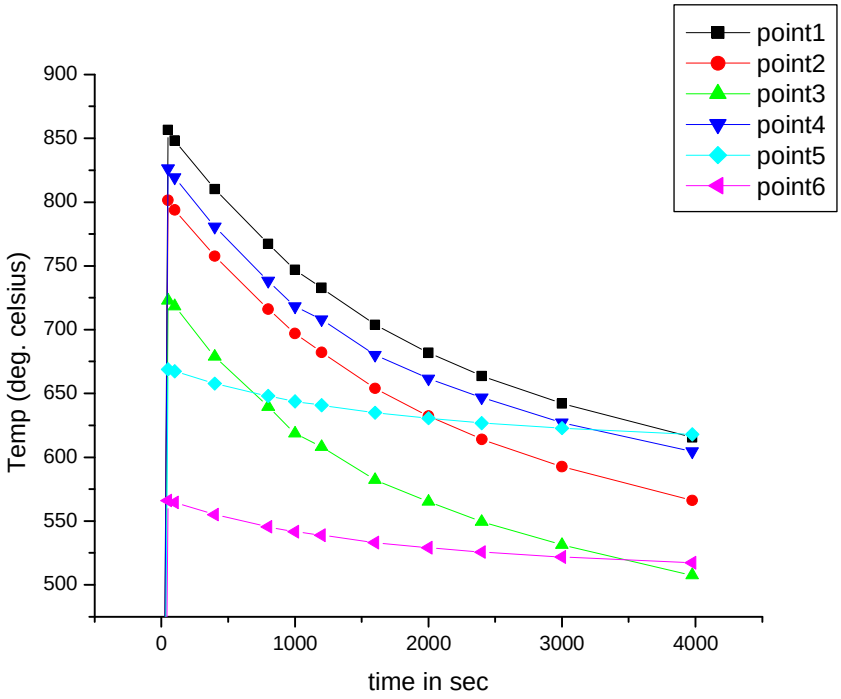

Fig 20 : Temperature profile for coupon 2 at various points of measurement

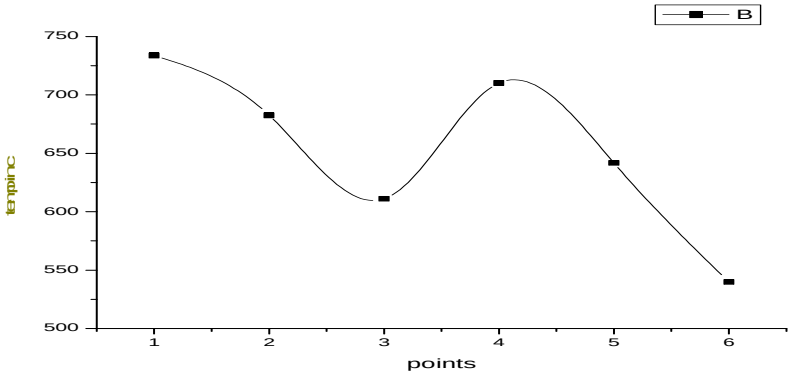

Fig 21: Mean temperature profile for coupon 2 at various points of measurement

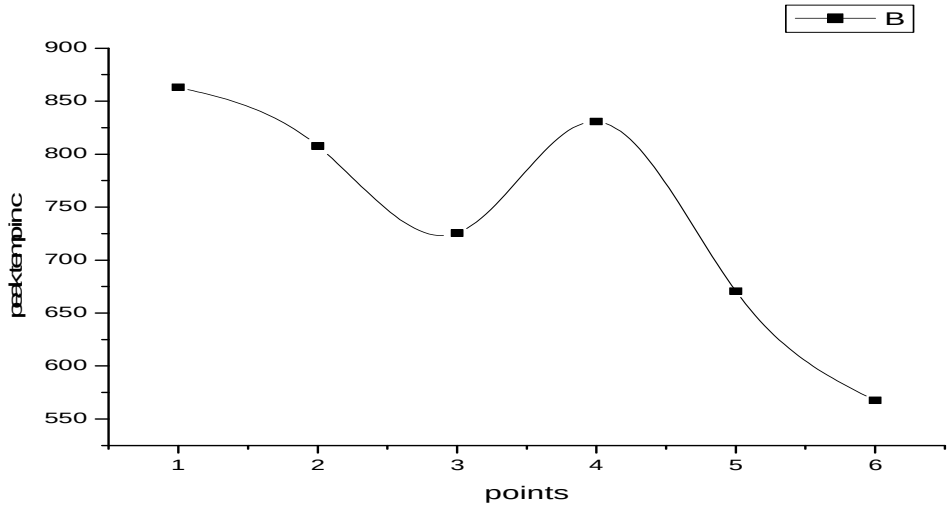

Fig 22: Peak temperature profile for coupon 2

5.1.1.1 DISCUSSION ON TEMPERATURE PROFILE

Fig 17 & Fig 18 shows the temperature profile of the coupon 1 and coupon 2.the maximum value of temperature measured during the welding by thermocouple in coupon 1 at point 1 near the mild steel HAZ because of high current density which results into production of high heat intensity source .similarly high value is observed in coupon 1 near SS weld as compared to coupon 2.

5.1.2 TENSILE TEST RESULT

Fig 23-25 shows the load versus displacement curves for weld coupons 1,2.The mechanical properties such as such yield strength, ultimate strength are calculated ultimate tensile strength are shown in table 11 weld coupon 1 had less UTS because of the defects found in the weld metals . Tensile strength and UTL of coupon 2 is more than coupon1

Table 11: Tensile test result for weld coupons

Weld coupon	UTL(KN)	% elongation
Weld coupon 1	80.4	9
Weld coupon 2	86.4	11
MS BASE	52.5	8.5
SS BASE	85.3	6.5

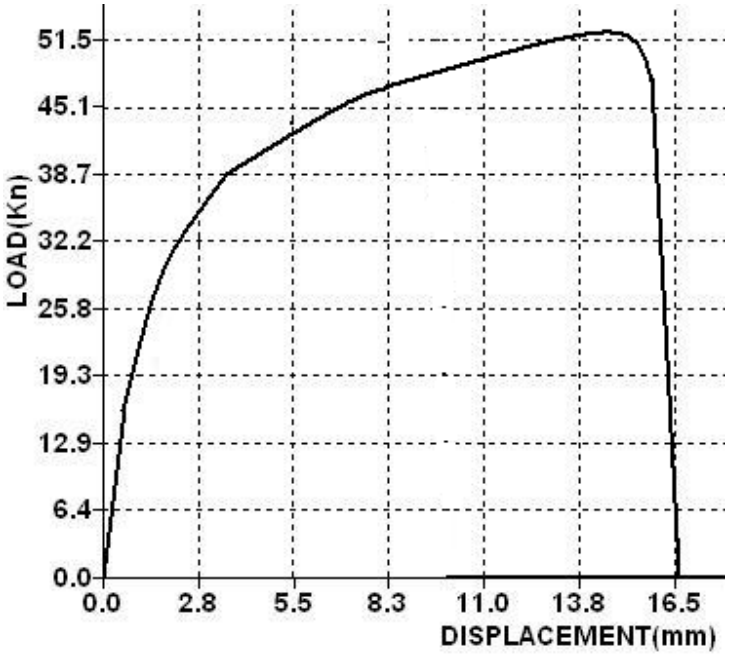

Fig 23. Load displacement graph for MS base

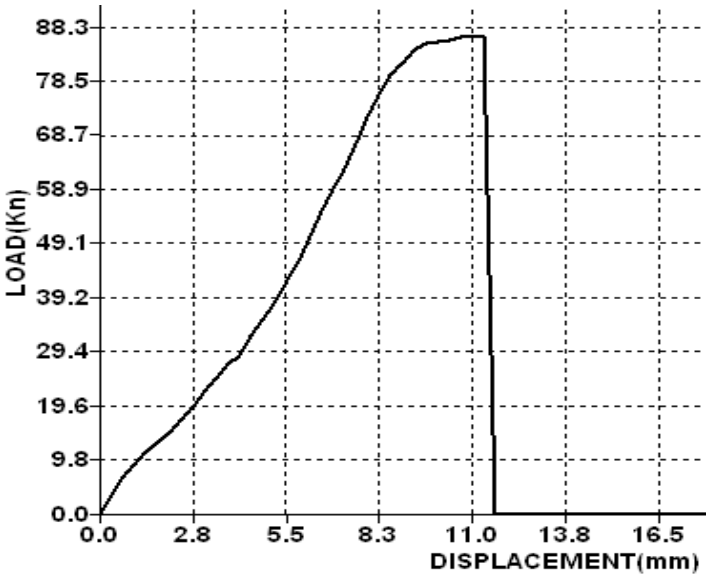

Fig 24. Load displacement graph for SS base

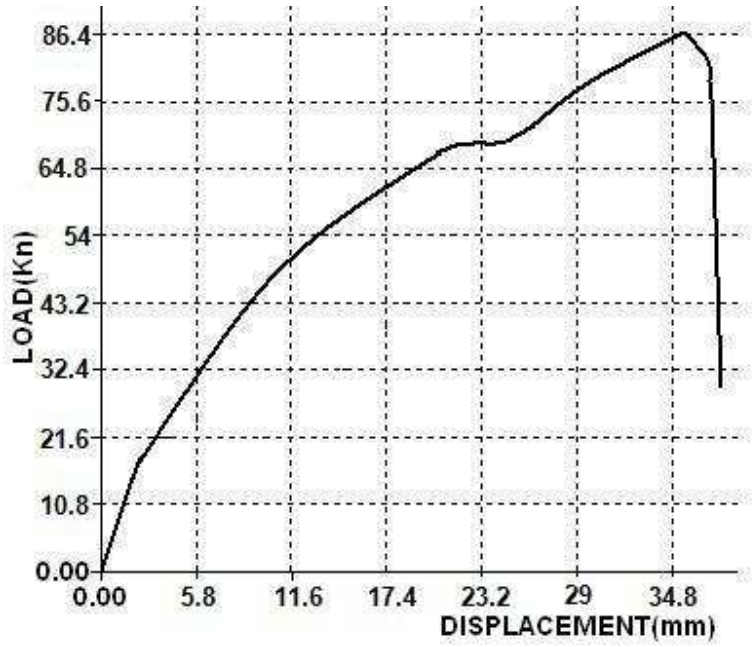

Fig 25. Load displacement graph for coupon 2

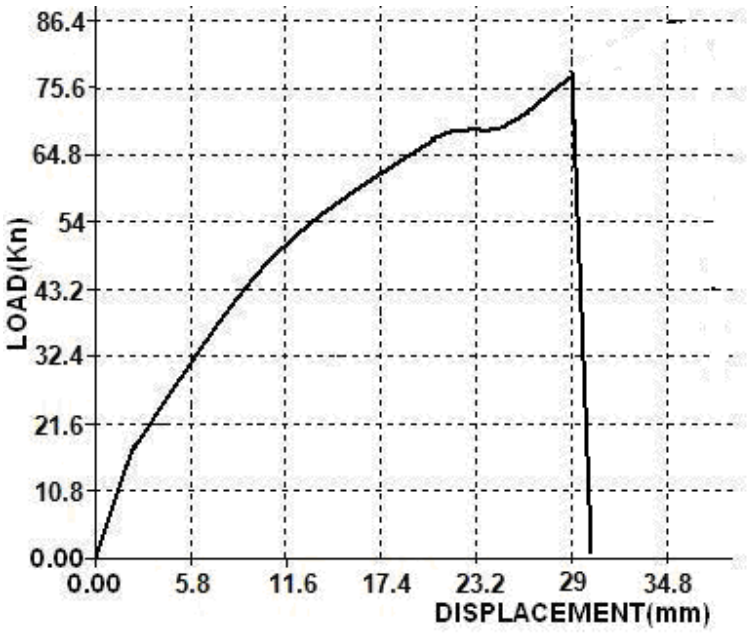

Fig 26.1 Load displacement graph for coupon 1

5.1.2.1 DISCUSSION ON TENSILE TEST RESULTS

Figs.23-26 show the load versus displacement curves for weld coupons 1 & 2. The mechanical properties such as ultimate tensile strength and percentage elongation are calculated are shown in table 11.weld coupon 1 had less UTS as compared to coupon 2 Because of defects found in the weld metals. In coupon 1 there is inverse relation ship between microhardness and UTL

5.1.3 IMPACT TOUGNHNESS RESULT

Table 12. Measured toughness of weld coupon 1

Temperature in °c	Toughness in Nm
40	134.8875
-10	120.1725
-30	98.1
-40	73.575
-45	58.86
-50	34.335

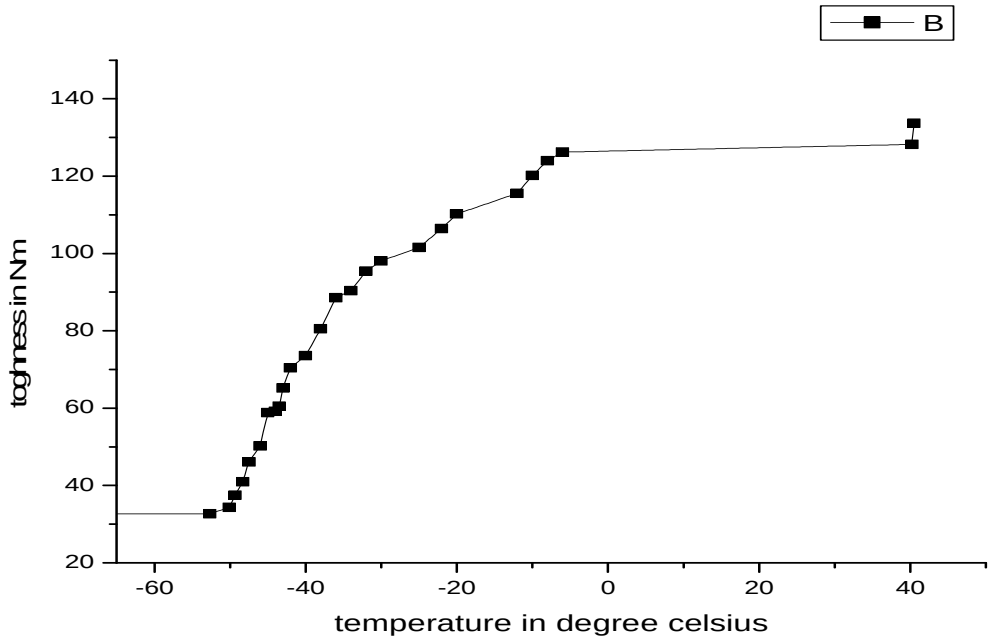

Fig 27 : Toughness of weld coupon 1

Table 13. Measured toughness of weld coupon 2

Temperature in °c	Toughness in Nm
40	117.72
-10	103.00
-30	63.765
-40	44.145
-45	36.7875
-50	32.0725

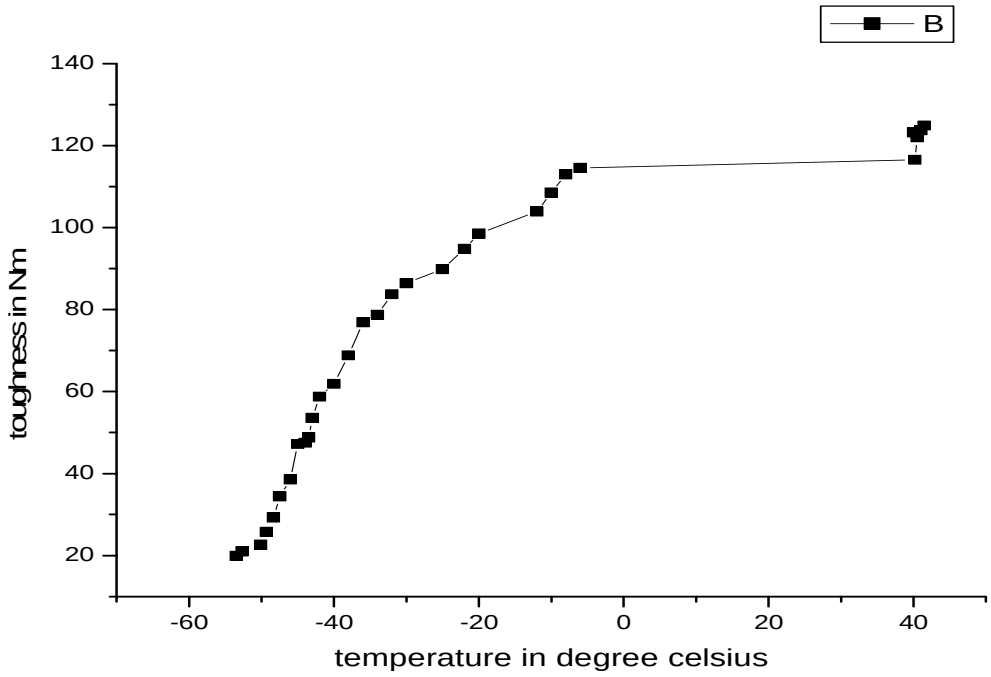

Fig 28: Toughness of weld coupon 2

5.1.3.1 DISCUSSION ON IMPACT TOUGHNESS

Figs shows the measured values of impact toghness at different temperature room temperature,-10°c,-30°c,-40°c,-50°c.At room temperature coupon 1 has maximum toughness as compared to coupon 2. it is also observed that at -50°c Coupon 1 has maximum value i.e 134.335

5.2.1 RESIDUAL STRESS MEASUREMENT

Any residual stress created by the selected drilling method will adversely affect the accuracy of result, a verification of the selected process was done. In this a strain gauge rosette, which used in the test, was applied to a stress free specimen of the same nominal composition and a hole drilled in the center of the rosette. From the measured strains, residual stresses were calculated by the following ASTM –E837 standard.

In order to measure longitudinal and transverse residual stress tests were performed on weld coupon. The measured strains in each trial were tabulated in table 8 & table 9 for coupon 1 &coupon 2.

Table 14. Shows values of longitudinal stresses & transverse stresses of coupon 1

points	Longitudinal stress(Mpa)	Transverse stress(Mpa)
1	-66.4383	386.3783
2	20.86601	265.7854
3	-443.319	-468.301
4	-412.706	-331.273

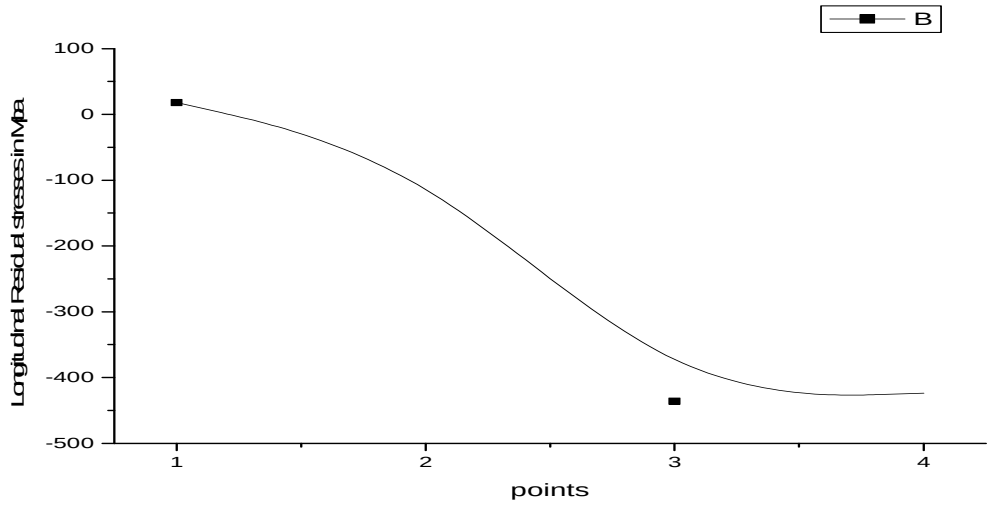

Fig 29: Longitudinal residual stresses for coupon 1

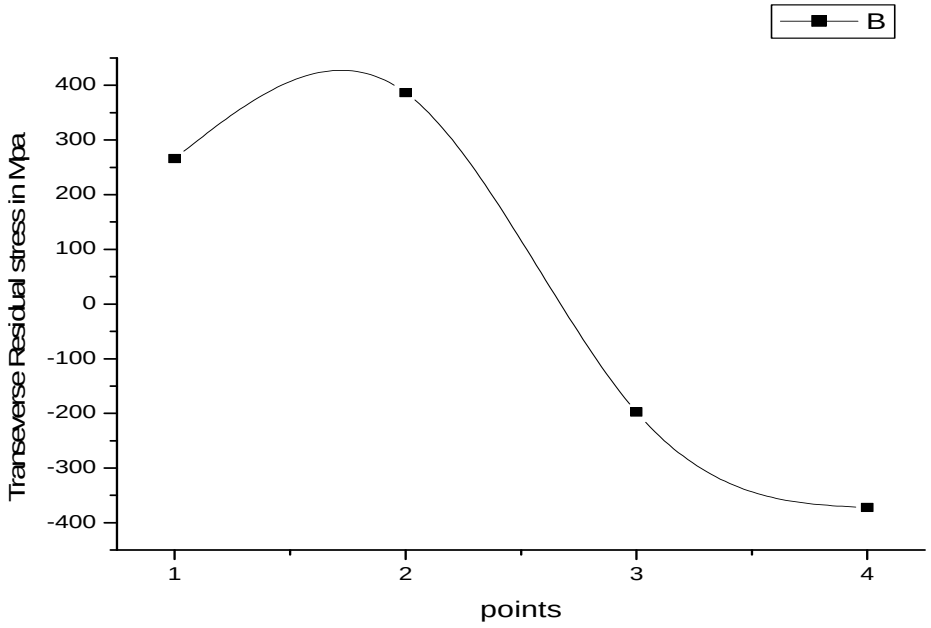

Fig 30: Transverse residual stresses for coupon 1

Table 15: Longitudinal stresses & Transverse stresses for coupon 2

points	Longitudinal stress(Mpa)	Transverse stress(Mpa)
1	18.06896	265.8792
2	-62.6704	376.6313
3	-435.925	-197.374
4	-423.741	-372.005

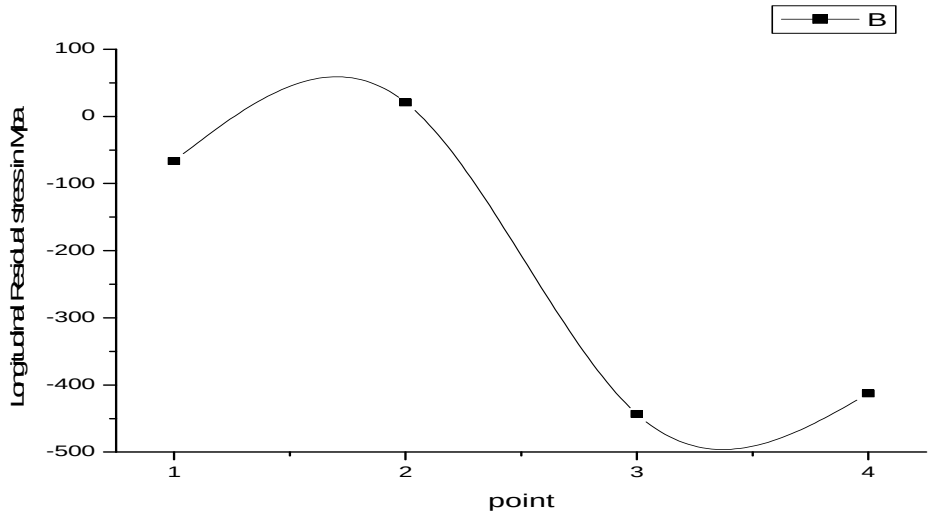

Fig 31: Longitudinal stresses for coupon 2

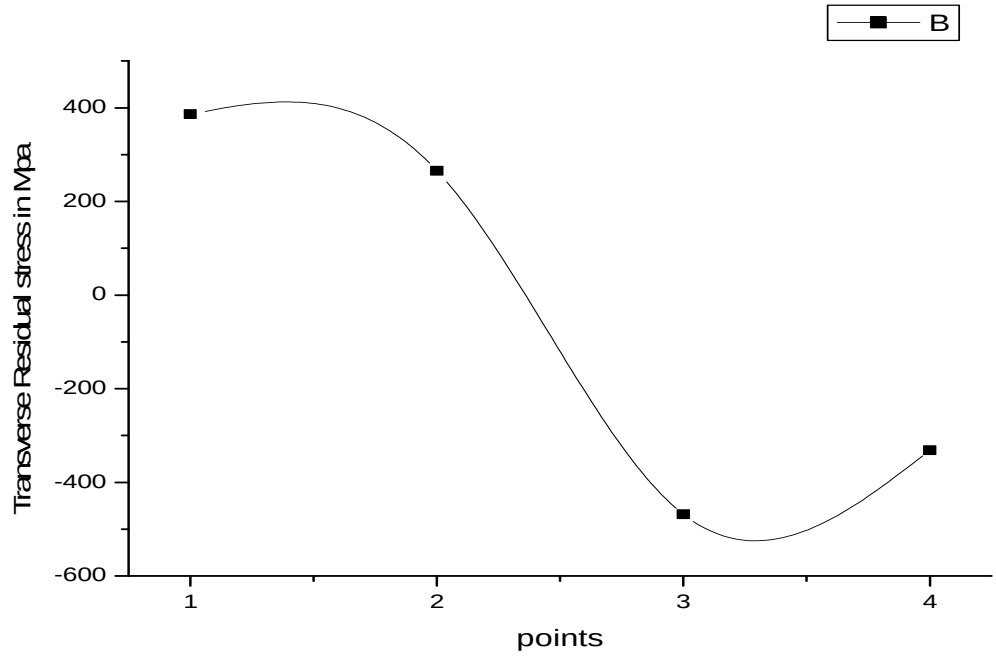

Fig 32 : Transverse stress for coupon 2

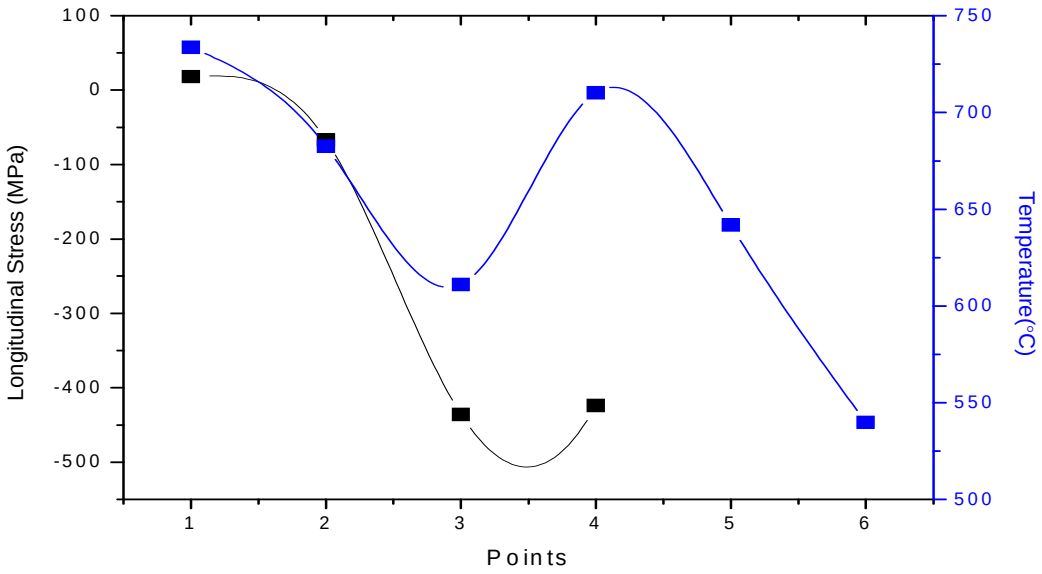

Fig 33: Relation between longitudinal stresses & temperature at different points of coupon 1

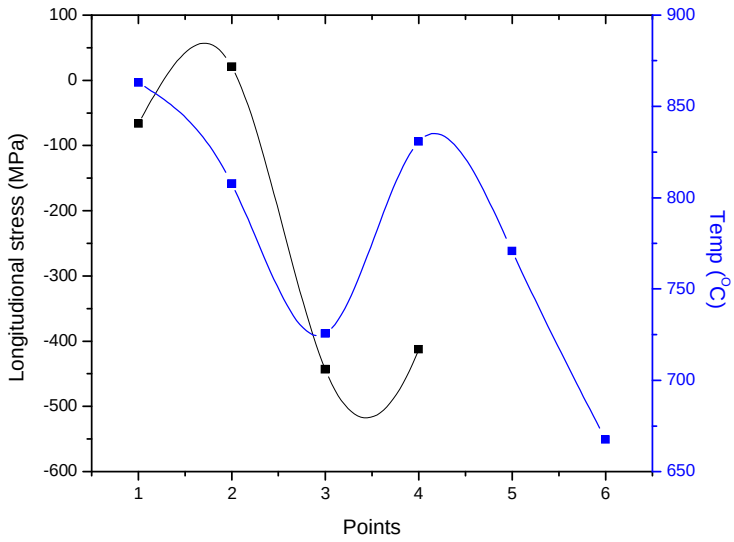

Fig 34: Relation between longitudinal stresses & temperature at different points in coupon 2

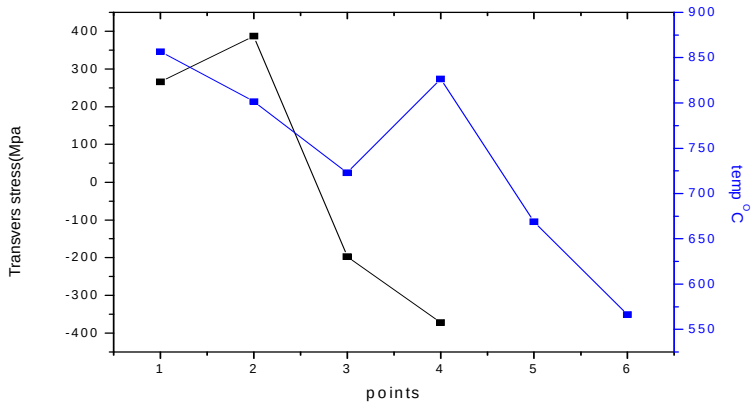

Fig 35: Relation between transverse stresses & temperature at different points in coupon 1

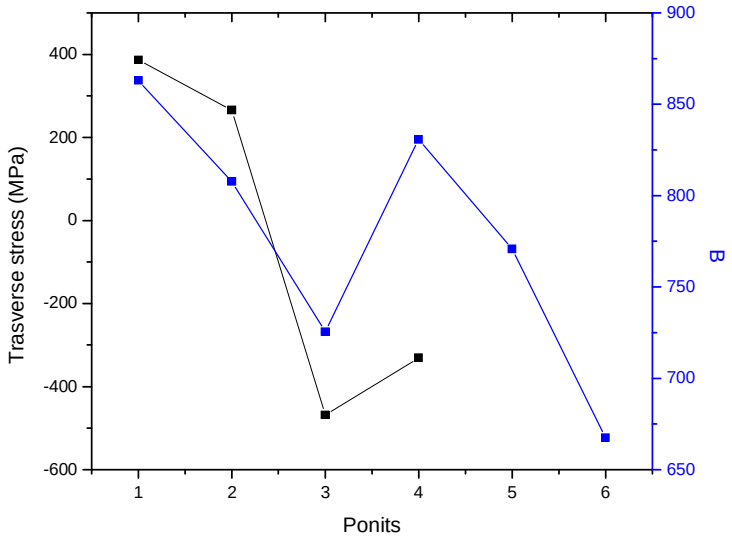

Fig 36: Relation between transverse stresses & temperature at different points in coupon 2

5.2.1.1 DISCUSSION ON RESIDUAL STRESS MEASURE MENT

Longitudinal and transverse residual stress are given in tables 14 & table 15 points 1,2,3&4 indicate mild steel HAZ mild steel base ,SS weld & SS base in coupon 1 & coupon 2.Points 1,2,3 &4 mild steel HAZ, mild steel base ,SS base & SS HAZ. Mild steel base and SS steel base points are taken at 15 mm from weld center. Mild steel HAZ & SS HAZ point are taken 10 mm from weld center.

Longitudinal stress is observed maximum in weld coupon1 at mild steel base. this due to less carbon migration from mild steel to weld metal longitudinal stress. value of transverse stress in coupon 1at mild steel HAZ is also maximum.Value of transeverse stress is observed maximum at SS HAZ except coupon 2.these higher values may be because of the the low thermal conductivity and high thermal expansion coefficient of austenitic stainless steel when compared to mild steel. Fig 33 to fig 36 shows the relation ship between temperature and residual stress of coupon 1 coupon 2.It shows when the temperature is increased residual stress is also increased.

5.3 CHEMICAL COMPOSITION

Table 16 . Chemical composition of coupon 1 at different weld regions

REGION	Fe	C	Si	Mn	Cr	Ni	Mb
SS BASE	44.1	1.12	4.5	4.05	22	13.4	0.324
SS WELD	33.2	0.555	2.99	7.35	35	9.77	0.0984
BUTTERING	45.5	4.26	1.79	2.92	28.9	10.8	0.0553
MS HAZ	80.8	0.441	1.38	4.4	0.108	0.922	0.109
MS BASE	80.2	0.345	1.37	4.3	0.092	0.845	0.105

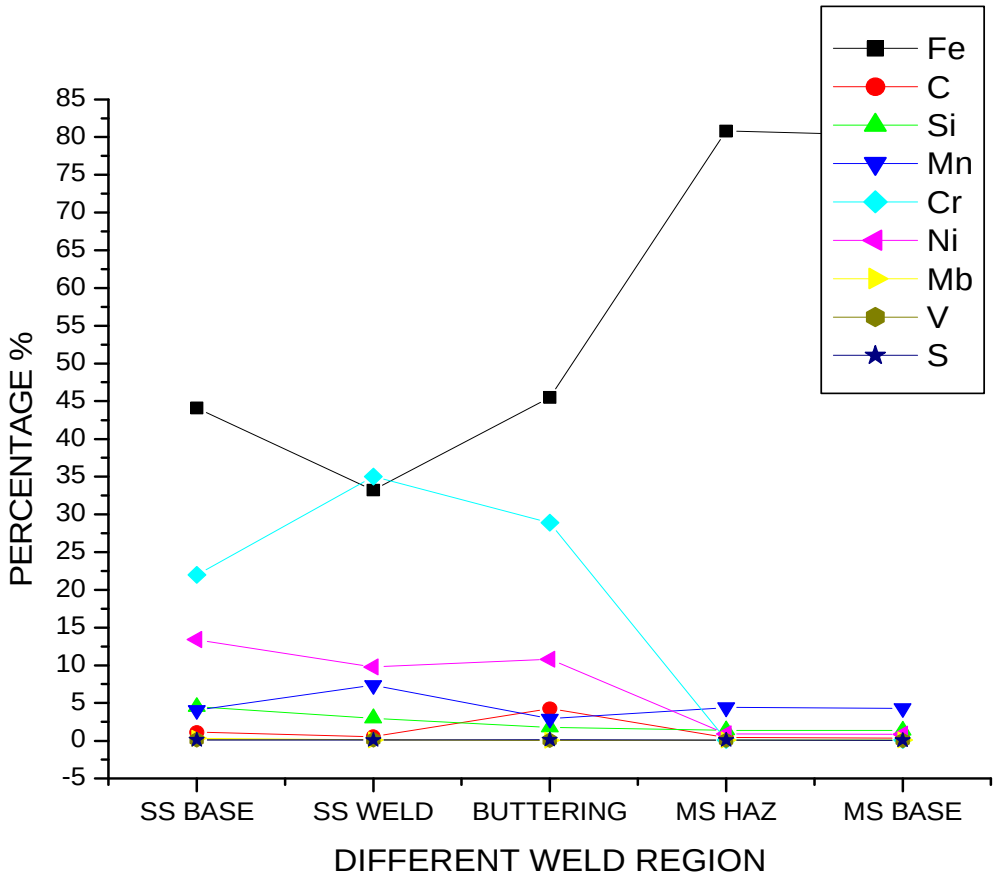

Fig 37. Percentage of Chemical composition of coupon 2 at different weld regions

Table 17. Chemical composition of coupon 2 at different weld regions

REGION	Fe	C	S	Mn	Cr	Ni	V
SS BASE	44.1	1.12	0.103	4.05	22	13.4	0.123
SS WELD	36.6	0.36	0.125	6.41	33.9	11.4	0.0607
BUTTERING	31.8	0.0862	0.0417	8.09	35	7.79	0.0865
MS HAZ	67.3	1.13	0.15	3.07	0.151	9.92	0.093
MS BASE	80.2	0.345	0.142	4.3	0.092	0.845	0.0957

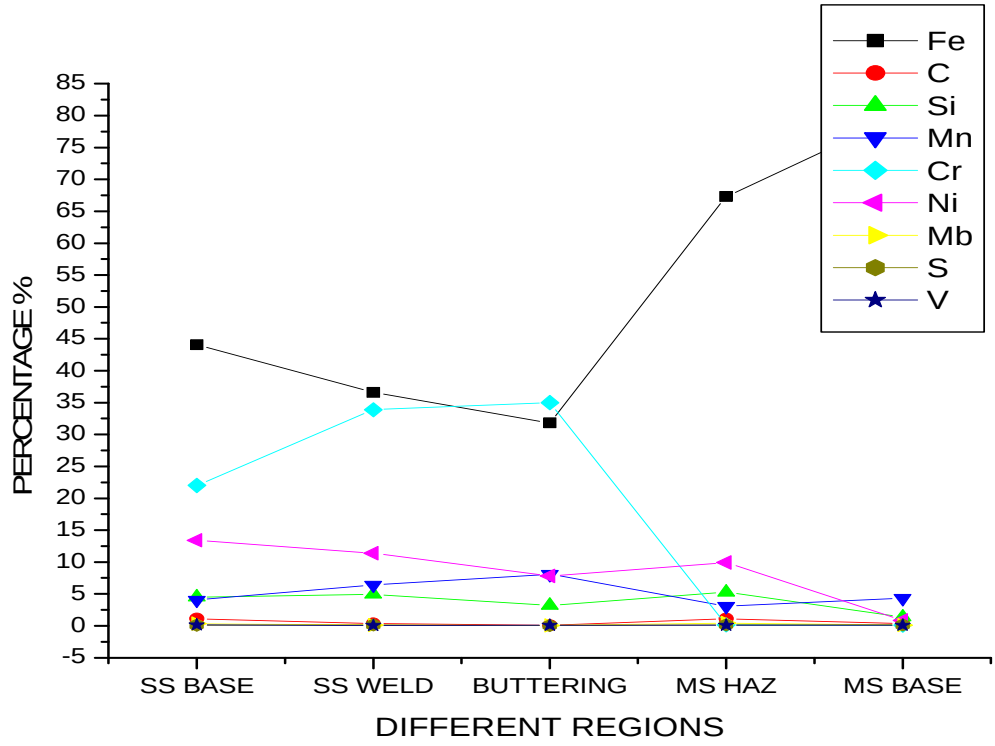

Fig 38. Percentage of Chemical composition of coupon 2 at different weld regions

5.3.1 DISCUSSION ON CHEMICAL COMPOSITION

Fig 37 and fig 38shows the result of percentage changes of composition in coupon 1 & coupon 2. The graphs in Figure 37-38 show the element percentage composition and element percentage change for MS, Interface and SS regions of friction welded joints. In coupon 1 percentage of carbon is decreased abruptly as compared to change in percentage of carbon in coupon 2. This is due to high carbon migrating from mild steel base to weld zone as compared to coupon 2.value of change in percentage of sulpur & vanadium is constant.

5.4 MICROSCOPIC BEHAVIOUR

Result of experiment performed is discussed in this chapter which includes micro hardness ,microstructure at various points in weld coupons, tensile test.

5.4.1 MICROHARDNESS

Micro hardness were taken along a line in the middle of the thickness of the specimens and included base metals, the heat affected zones(HAZ),fusion line ,buttering layer & weld area . Maximum value of micro hardness in coupon 1 was observed in SS HAZ where it is maximum in other coupon this may be due to carbon prevented by buttering layer from migrating from stainless steel to weld zone.

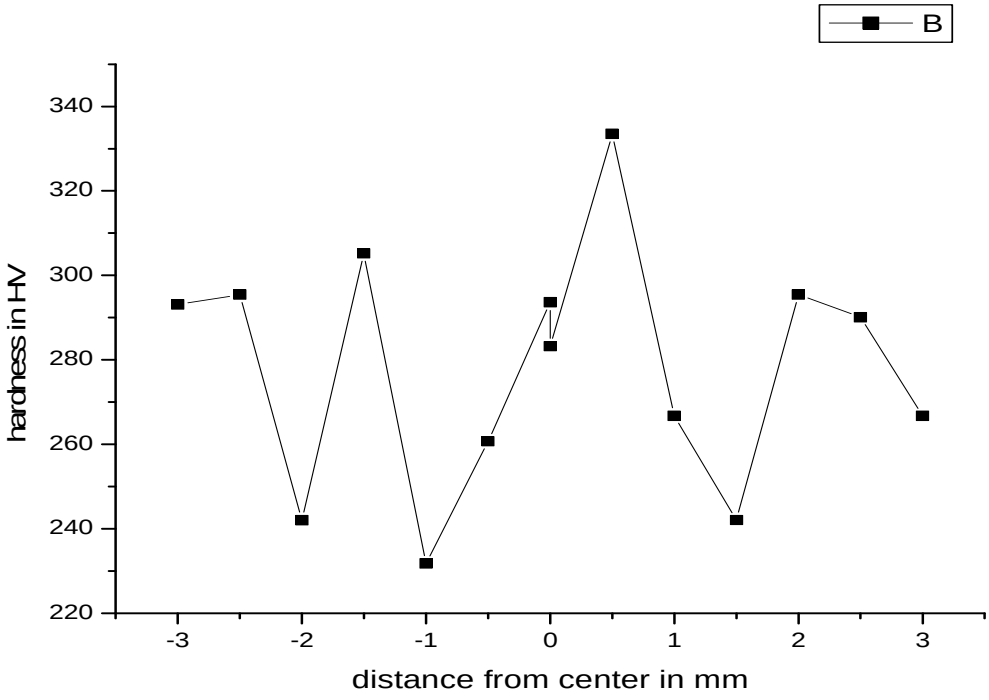

Fig 39: Micro hardness in longitudinal direction of the weld coupon 1

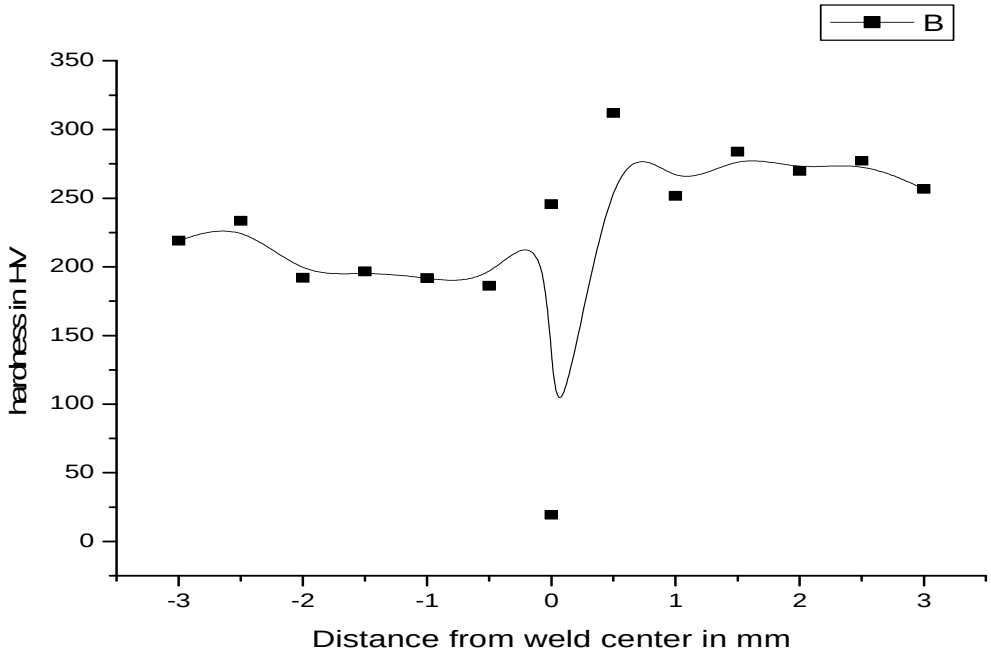

Fig 40: Micro hardness in longitudinal direction of the weld coupon 2

5.4.1.1 DISCUSSION ON MICRO HARDNESS

Fig 39 and fig 40 shows the result of micro hardness test . There were taken along the interface line & included base metal ,the heat affected zone ,fusion line, weld area. it shows maximum value of micohardness is observed in coupon 1 in the weld zone & MS fusion line this may be due to the carbon prevented by the buttering layer mild steel to weld zone .

5.5 MICROSTRUCTURE

1

2

3

4

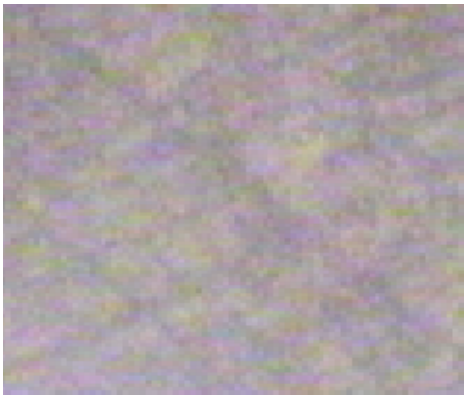

5

6

Fig 41: Microstructure of weld coupon 1 at interface

1 2

Fig 42 : Microstructure of weld coupon 1 at german steel base

3 4

Fig 43: Microstructure of weld coupon 1 at stainless steel base

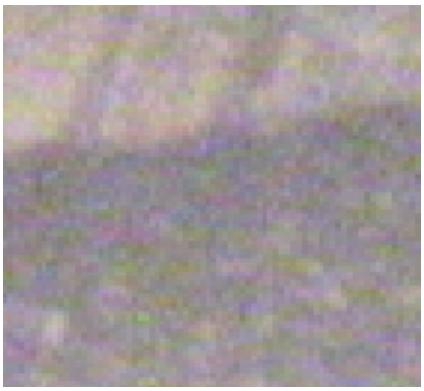

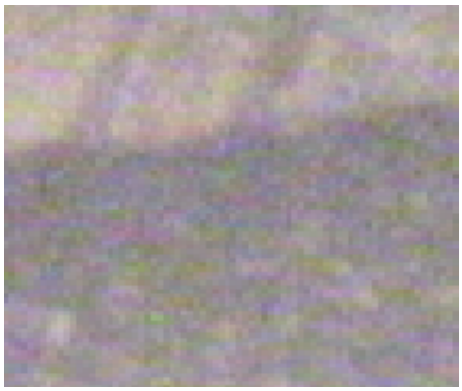

Fig 44: Microstructure of weld coupon 2 at interface

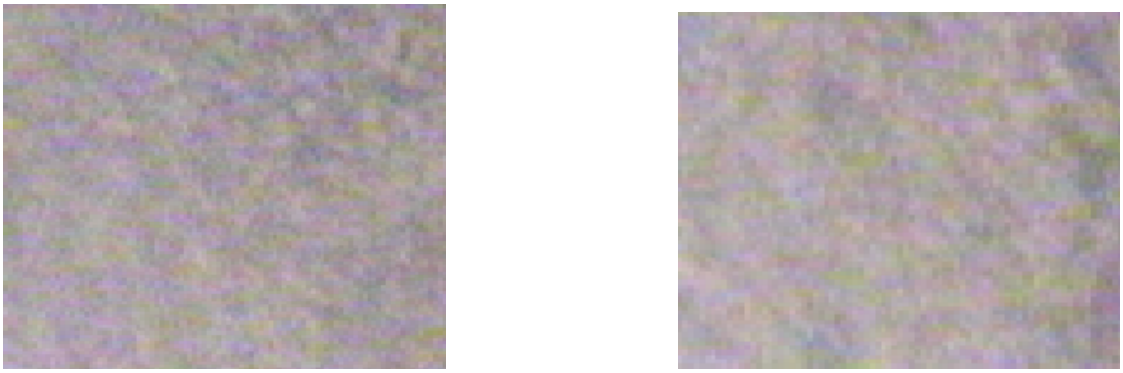

Fig 45: Microstructure of weld coupon 2 at german steel

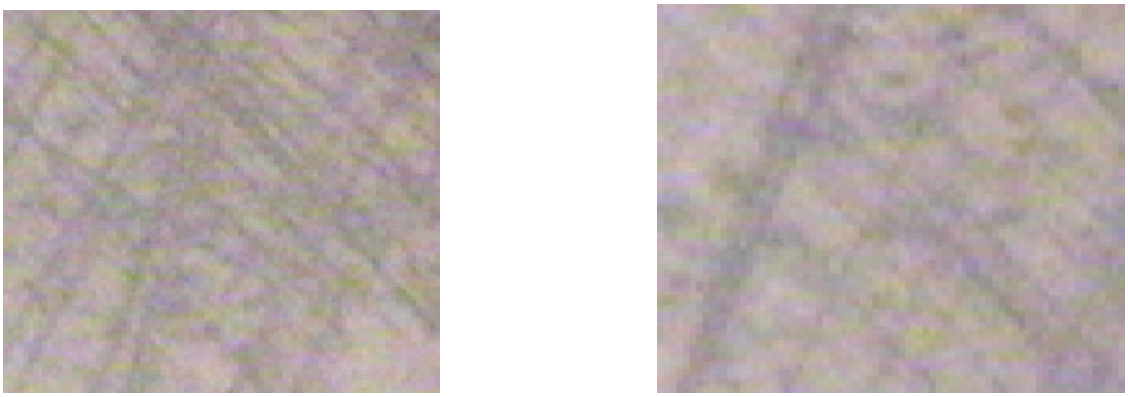

Fig 46: Microstructure of weld coupon 2 at stainless-steel

5.5.1 DISCUSSION OF OPTICAL MICROSTRUCTURE:

Base Material: The microstructure of mild steel base at magnifications of 400X is shown in figs .The micro-graph of the figures reveal the presence of typical ferrite (bright)-pearlite (dark) microstructure. The density of flow lines i.e. banding and the morphology of ferrite and pearlite has been found to vary in samples. The microstructure of stainless steel base at magnifications of 400X is shown in Figure 43 &46. The austenitic grains are clearly visible in the microstructure.

Weld Metal

Two microstructural regions featured by cast dendrite and reheat refined grains as shown in in the interface Figures. The reheat refined region closed to the dendritic boundary develops comparatively coarser grain than the size observed in the reheat refined region away from the dendritic boundary of the interface. Therefore it can be said that the

distribution of the microstructure in the weld consists of three distinctly different microstructural regions, such as the dendritic region at interface (D), reheat refined coarse grain region (RC) and reheat refined fine grain region (RF). The microstructures of the different interface regions of weld metal as revealed in the TIG weld are typically shown in the micrographs presented in Figures 41 & 44. The distribution of the three different microstructural regions has been found to be similar in all the welds.

The morphologies of the dendritic region at interface (D), coarse grain reheat refined region in MS HAZ (RC), and the grain reheat refined region (RF) in SS HAZ of all the welds have been comprehensively studied at different magnifications under optical microscope. The studies on these three regions of the welds have been typically shown in all Figures. The micrographs depict that the dendritic region (D) is possibly having lower bainite in combination of some amount of fine pearlite with pro-eutectoid ferrite at the grain boundary . The coarse grain reheat refined region (RC) primarily contains austenite and a mixture of acicular and chunky ferrite whereas, the fine grain reheat refined region MS HAZ has been found to primarily consists of ferrite and pearlite . The variation in coarseness of the morphology of different welds, as revealed in the weld joints, inherently occurs at different locations of different welds depending upon randomness and heterogeneity in distribution of weld temperature cycle. Thus, it may be concluded that the morphology of the weld prepared varies within a broad range of coarseness as typically marked in the micrographs presented in the Figures.41-46.

CHAPTER 6 CONCLUSION & SCOPE OF WORK

6.1 CONCLUSION

(1) Residual stresses were measured using hole drilling techniques . longitudinal stress in weld coupon 1 is maximum in mild steel HAZ & stainless steel HAZ. Longitudinal residual stress at mild steel 15 mm from the centre line is maximum of coupon 1.values of transverse residual stress is also maximum in coupon 1 as compared to coupon 2 in mild steel HAZ. It can be concluded that coupon 1 was welding with current 220 amp which results into more heating produce compare with coupon 2 which was welded with welding current of 180 ampere.Higher peak temperature result in higher residual stress.

(2) Temperature measured during the welding of coupon 1 was maximum recorded as compared to coupon 2 due to high intensity of heat source .

(3) The mechanical properties such as ultimate strength, % elongation were measured in tensile testing .coupon 1 has less UTS ,UTL.

(4) Micro hardness were taken along the interface line & included base metal heat affected zone ,fusion line, weld area.Maximum value of micohardness is observed in coupon 1 in the weld zone & MS fusion line this may be due to the carbon prevented by the buttering layer mild steel to weld zone .

(5) Impact strength at room temperature coupon 1 has maximum value as compared to coupon 2. it is also observed that at -50°c Coupon 1 has maximum value i.e 34.335.

(6) The chemical composition of coupon 1 percentage of carbon is decreased abruptly as compared to change in percentage of carbon in coupon 2. this is due to high carbon migrating from mild steel base to weld zone as compared to coupon 2.Value of change in percentage of sulpur & vanadium is constant.

(7) The variation in coarseness of the grain morphology of different weld microstructure, as revealed in the weld joints, inherently occurs at different locations of different welds depending upon randomness and heterogeneity in

distribution of weld temperature cycle. Thus, it may be concluded that the morphology of the weld prepared varies within a broad range of coarseness

6.2 SCOPE OF FUTURE WORK

Strain gauge hole drilling techniques for residual stress measurement involves some operation which requires very high level of accuracy such selection of adhesive proper pasting of strain gauge rosettes and their orientation, drilling operation with constant speed. Vibration involved in drilling operation should be taken care of. These factors affect the accuracy of the method, so number of tests can be performed or it can be supported by other method.

Residual stress study can also be done with different groove designs, differents welding parameter , different materials(similar or dissimilar and different buttering layers

REFRENCES

(1) Dean Deng, Yu Luo, Hisashi Serizawa, Masakazu Shibahara, Hidekazu Murakawa, JWRI 32 (2) 2003, 325-333.

(2) Radaj D., Welding Residual Stresses and Distortion Calculation and MeaS\lrement, DVS, Verlag, 2003, ISBN 3-87155-791-,9.

(3) Davis S.R., Hard facing, weld cladding and dissimilar metal joining, Welding, brazing and soldering, ASM Handbook, vol. 6. Ohio, ASM International, 1993, pp. 789-829.

(4) Klueh R.L., King J.F., Austenitic-ferritic weld joinffailures', Welding Journal, 1982, 61,302s--311s.

(5) Emerson R.W., Hutchinson W.R., Welded joints between dissimilar metals in high temperature service, Welding Journal 1952, 31, 126s-141 s.

(6) Thielsch H., Stainless steel weld deposit on mild steel and alloy steels, Weld . .I. 1952, 31,37s-664s.

(7) Joseph A, Ramesh A.S., Jayakumar T, Murugan N., Failure analysis of a dissimilar weld joint in steam generator, Pract Metallograph 2001,38(12).

(8) Thielsch H., Stainless steel weld deposit on mild steel and alloy steels, Weld. J. 1952, 31,37s-664.

(9) Rutherford J .lB., Welding stainless steel to c2,rbon or ferritic steel, Weld. J. 1959, 38,19s-226.

(10) Rowley T, Rowberry T.R., Alldridge c., Problems associated with the design, inspection and use of large diameter ferritic/austenitic joints in power plant, proceedings of international conference welding dissimilar metals, Weld. J. 1969, 1(12s),13-17.

(11) Christoffel R.J., Curran R.M., Carbon migration welded joints at elevated temperatures, Weld. J. 1956, 35,457s-469.

(12) Klueh R.L., The effect of carbon on 2.25Cr-l Mo steel (I) microstructure and tensile properties . .I. Nuclear Mater 1974, 54,41-54.

(13) Lundin C.D., Dissimilar metal welds-transition joints literature review, Weld . .I. 1982,61, 58s-663.

(14) Klueh R.L, King J.F, Griffith J.L., A simple test for dissimilar-metal Welds,

Welding Journal, 1983,62, 154s-19s. (15) Davis S.R .. , Hard facing, weld cladding and dissimilar metal joining, welding brazing and soldering, In, ASM handbook, vol. 6. Ohio, ASM International, 1993, pp.789-829.

(16) Dissimilar metals, Welding Handbook. i^{h} ed. vol. 4, Miami, American Welding Society, 1992, pp. 514-47.

(17) Singh Raman R.K.., Role of microstructural degradation in the heat affected zone of 2.25Cr-lMo steel weldments and sub scale features during steam oxidation and their role in weld failures. Metallurgical Material Transaction A 1998, 29A (2), 577-86.

(18) Tucker J.T., Eberle F., Development of a ferritic-austenitic weld joint for steam plant application. Welding Journal, 1956,35, 529s-540.

(19) Bruscato R., Temper embrittlement and creep embrittlement of 2.25Cr-IMo shielded metal arc weld deposits, Weld. J. 1970, 49,148s-156.

(20) Swift R.A, Gulya J.A., Temper embrittlement of pressure vessel steels, Weld. J. 1973, 52,57s-668.

(21) Eckel J.F., Diffusion across dissimilar metal joints. Welding Journal, 1964, 43, 170s-18.

(22) Roschin V.V., Residual stresses in pipe joints between dissimilar steels, Weld Prodn.1969,9,55-8.

(23) Pang C.S., Pukas M.W., Park J.H., Investigation of welding residual stress of high tensile steel by fi nite element method and experiment, KSME Int. J. 13 1999 879-885.

(24) Chandra B.D., A numerical thermo-mechanical model for the welding and subsequent loading of a fabricated structure, Comput. Struct. 3, 1973, 1145-1174.

(25) Brand 1.B., Determination of residual stresses in submerged arc multi-pass welds by means of numerical simulation and comparison with experimental measurements, Welding World 33,1994,152-159.

(26) S.L. Chu, H. Peukrt, E. Schnider, Residual stress in a welded steel plate and their measurement using ultrasonic techniques, MRL Bulletin Research Development 1 (2), 1987,45-50.

(27) M. Leoni, P. Scardi, S. Rossi, L. Fedrizzi, Y. Massiani, (Ti,Cr)N and TiiTiN PVD coating on 304 stainless steel substrates, texture and residual stress, Thiri Solid Films 345, 1999,263-269.

(28)Murugan S.,Rai S.K,Kumar P.V.,Jayakumar T .,Baldev Raj,BoseM.S.C.,International journal of pressure Vessel and piping 78,2001 307-317.

(29)Brickstad B.,Josefson B.L.,International Journal of pressure vessel and piping 75,1998,11-25

(30)Dean Dang ,Hidekazu murukawa,Numerical simulation of temperature field and residual stress in multi-pass welds in stainless steel pipe and comparisoin with experimental measurement ,weld.j.1957,35,457s-469.

(31)Murugan s.,Kumar P.V.,Baldev Raj,Residual stress analysis in weldments, theortical Approach ,Indian Welding journal,vol.29(4),1996,pp7-23

(32) Masubuchi K.,Analysis of welded structure .residual stress

(33) Kasatkin BS, et al. Experimental methods of investigation of strains and stresses. Kiev: Naukova Dumka; 1981. 583 p.

(34) Kobayashi A, editor. Experimental mechanics. Vol. 2.Moscow: 1990. 551 p. Birger IA. Residual stresses in structural members. Residual technological stresses. Moscow: 1985. p. 5–27.

(35) Lobanov LM, Pivtorak VA. Development of holographic interferometry for the investigation of the stress-strength state and inspecting the quality of welded joints.In: Advanced materials for the 21st-century. Kiev: Naukova Dumka; 1998. p. 620–636.

(36) Lobanov LM, et al. Efficient inspection of the quality and determination of residual stresses in welded structures by electronic speckle interferometry. Avt Svarka. 2005;8:10–13.

(37) Moore AJ, Tyrer JR. Two-dimensional strain measurement with ESP. Optical Laser Engineering. 1996;24:381–402.

(38) Zhang J. Two-dimensional in-plane electronic speckle pattern interferometer and its application to residual stress determination. Optical Engineering. 1998;37:2402–2409.

(39) Sirohi RS, editor. Speckle metrology. New York: Marcel Decker; 1993.
(40) Makino A, Nelson D. Residual stress determination by single-axis holographic interferometry and hole drilling, part I, Theory, Exp. Mech. 1994;34:66–78.
(41) Wu Z, et al. Study of residual stress distribution by moiré interferometry incremental hole drilling method. In: Fifth International conference on residual stresses. Sweden: Linkoping; 1997.
(42) Schaer GS. Application of the finite element calculations to residual stress measurements. J. Eng. Mater. Tech.1981;103(4):157–163.
(43) Timoshenko SP. Lectures in the theory of plasticity. Kiev: Naukova Dumka; 1972. 501 p.
(44)M. Mochizuki, "Control of Welding Residual Stress for Ensuring Integrity Against Fatigue and Stress–Corrosion Cracking," Nucl. Eng. Des., 237, p. 107 (2007).
(45) P. Michaleris, J. Dantzig, and D. Tortorelli, "Minimization of Welding Residual Stress and Distortion in Large Structures," Welding J., 78, p. 361s (1999).
(46) E. B. Bartlett and R. E. Uhrig, "Nuclear Power Plant Diagnostics Using an Artificial Neural Network," Nucl. Technol., 97, p. 272 (1992).
(47) H. G. Kim, S. H. Chang, and B. H. Lee, "Optimal Fuel Loading Pattern Design Using an Artificial Neural Network and A Fuzzy Rule-Based System," Nucl. Sci. Eng., 115, p. 152 (1993).
(48) K. Kavaklioglu and B. R. Upadhyaya, "Monitoring Feedwater Flow Rate and Component Thermal Performance of Pressurized Water Reactors by Means of Artificial Neural Networks," Nuclear Technology, 107, p. 112 (1994).
(49) J. W. Hines, D. J. Wrest, and R. E. Uhrig, "Signal Validation Using an Adaptive Neural Fuzzy Inference System," Nucl. Technology, 119, p. 181 (1997).
(50) P. Fantoni, S. Figedy, and A. Racz, "A Neuro-Fuzzy Model Applied Full Range Signal Validation of PWR Nuclear Power Plant Data," FLINS'98, Antwerpen, Belgium, Sept. 14-16, 1998.
(51) M. G. Na and B. R. Upadhyaya, "A Neuro-fuzzy Controller for Axial Power Distribution in Nuclear Reactors," IEEE Trans. Nucl. Sci., 45, p. 59 (1998).

(52) M. G. Na, Dong Won Jung, Sun Ho Shin, Kibog Lee, and Yoon Joon Lee, “Estimation of the Nuclear Power Peaking Factor Using In-core Sensor Signals,” J. Korean Nucl. Soc., 36, p. 420 (2004).
(53) Hibbitt, Karlson & Sorensen, Inc., ABAQUS/Standard User’s Manual, 2001.
(54)V. Robin et al., “Modelling of Bimetallic Welds,” Proc. Mathematical Modeling of Weld Phenomena 6, 2002.
(55) D. E. Katsareas and A. G. Youtsos, “Residual stress prediction in dissimilar metal weld pipe joints using finite element method,” Proc. ICRS-7, 2004.
(56) B. Brickstad and B. L. Josefson, “A Parametric Study of Residual Stresses in Multi-Pass Butt-Welded Stainless Steel Pipes,” Int. J. of Press. Ves. & Piping, 75, p. 11
(1998). [14] S. L. Chiu, “Fuzzy Model Identification Based on Cluster Estimation,” J. Intell. Fuzzy Systems, 2, p. 267 (1994).
(57) T. Takagi and M. Sugeno, “Fuzzy Identification of Systems and Its Applications to Modeling and Control,” IEEE Trans. Systems, Man, Cybern., SMC-1, p. 116
(1985).
(58) M. G. Na, Neuro-Fuzzy Control Applications in Pressurized Water Reactors: in Da Ruan (ed) Fuzzy Systems and Soft Computing in Nuclear Engineering, Springer-Verlag, Berlin Heidelberg New York, pp. 172- NA et al., Prediction of Residual Stress for Dissimilar Metals Welding at Nuclear Power Plants Using Fuzzy Neural Network Models NUCLEAR ENGINEERING AND TECHNOLOGY, VOL.39 NO.4 AUGUST 2007 347 (a) Relative Error (b) Residual Stress Distribution for a Special Welding
Condition Fig. 8. Prediction Performance of Welding Residual Stress According to the Center Path Under Free Constraint at the End Section 207 (1999).
(59)D. E. Goldberg, Genetic Algorithms in Search, Optimization, and Machine Learning, Addison Wesley, Reading, MA (1989).
(60) M. Mitchell, An Introduction to Genetic Algorithms, MIT Press, Cambridge, MA (1996).
(61) “Effect of Weld Induced Residual Stresses on Pipe Crack Opening Areas and
Caterpillar (Caterpillar owned), exclusively distributed by Battelle Columbus Ohio, and The Welding Institute (TWI), Cambridge, England.

(62)Yang, Y, Brust, F. W., and Cao, Z., "Virtual Fab Distortion Predictions" in *Residual Stress, Fitness for Service, and Manufacturing Processes*, ed. F. W. Brust, proc 2003 ASME Pressure Vessels and Piping Conference, Cleveland, Ohio, USA, July 20-24, 2003

(63)Fredette, L., and Brust, F. W Implications on Leak-Before-Break Consiterations", in *Residual Stress, Fitness for Service, and Manufacturing Processes*, ed. F. W. Brust, proc 2003 ASME Pressure Vessels and Piping Conference, Cleveland, Ohio, USA, July 20-24, 2003.

(64)FRACALT© (Fracture Analysis Code via Alternating method), Version 2.0, January, 2001, Battelle Memorial Institute.

(65)Brust, F. W., 'The Importance of Material Fabrication History on Weld Durability and Fracture'.

(66) Mangyuna,jin weon kim and Dong hyuk,Lim Department of Nuclear Engineering ,chosun University fuzzy neural network model.

(67)L.M.Labonov,V.A.Pivotic,V.V.Savtiski.paton Electric Welding Institute ,Kiev ukrain